

***Some Recent Studies in Ruthenium Electrochemistry  
and Electrocatalysis***

N.S. Marinkovic\*, M.B. Vukmirovic and R.R. Adzic  
Department of Chemistry, Brookhaven National Laboratory, Upton, NY 11973.

*Submitted to Modern Aspects of Electrochemistry*

August 2006

**Chemistry Department**

**Brookhaven National Laboratory**

P.O. Box 5000  
Upton, NY 11973-5000  
[www.bnl.gov](http://www.bnl.gov)

Notice: This manuscript has been authored by employees of Brookhaven Science Associates, LLC under Contract No. DE-AC02-98CH10886 with the U.S. Department of Energy. The publisher by accepting the manuscript for publication acknowledges that the United States Government retains a non-exclusive, paid-up, irrevocable, world-wide license to publish or reproduce the published form of this manuscript, or allow others to do so, for United States Government purposes.

This preprint is intended for publication in a journal or proceedings. Since changes may be made before publication, it may not be cited or reproduced without the author's permission.

## **DISCLAIMER**

This report was prepared as an account of work sponsored by an agency of the United States Government. Neither the United States Government nor any agency thereof, nor any of their employees, nor any of their contractors, subcontractors, or their employees, makes any warranty, express or implied, or assumes any legal liability or responsibility for the accuracy, completeness, or any third party's use or the results of such use of any information, apparatus, product, or process disclosed, or represents that its use would not infringe privately owned rights. Reference herein to any specific commercial product, process, or service by trade name, trademark, manufacturer, or otherwise, does not necessarily constitute or imply its endorsement, recommendation, or favoring by the United States Government or any agency thereof or its contractors or subcontractors. The views and opinions of authors expressed herein do not necessarily state or reflect those of the United States Government or any agency thereof.

# Some Recent Studies in Ruthenium Electrochemistry and Electrocatalysis

N.S. Marinkovic<sup>\*</sup>, M.B. Vukmirovic and R.R. Adzic

Department of Chemistry, Brookhaven National Laboratory, Upton, NY 11973.

## 1. Introduction

Ruthenium is a metal of a considerable importance in electrochemical science and technology. It is a catalyst or co-catalyst material in Pt-Ru alloys for methanol- and reformate hydrogen-oxidation in fuel cells, while ruthenium oxide, a component in chlorine-evolution catalysts, represents an attractive material for electrochemical supercapacitors. Its facile surface oxidation generates an oxygen-containing species that provides active oxygen in some reactions. Ru sites in Pt-Ru catalysts increase the “CO tolerance” of Pt in the catalytic oxidation-reaction in direct methanol fuel cells (DMFC) and in reformate hydrogen-oxidation in proton exchange membrane fuel cells (PEMFC). The mechanism of Ru action is not completely understood, although current consensus revolves around the so-called “bifunctional mechanism” wherein Ru provides oxygenated species to oxidize CO that blocks Pt sites, and has an electronic effect on Pt-CO interaction.

While various studies of polycrystalline Ru go back several decades<sup>1,2,3</sup>, those involving single crystal surfaces and the structural sensitivity of reactions on Ru surfaces emerged only recently. Using well-ordered single crystalline surfaces brings useful information as the processes on realistic catalysts are far too complex to allow identification of the microscopic reaction steps. In this article, we focus on progress in model systems and conditions, such as electrochemistry and electrocatalysis on bare and Pt-modified well-ordered Ru(0001) and Ru(10 $\bar{1}$ 0) single-crystal surfaces. We also review current understanding of the mechanistic principles of Pt-Ru systems and a new development of a Pt submonolayer on Ru support electrocatalyst.

Ruthenium crystallizes in a hexagonal close-packed structure, (*hcp*). **Figure 1.1** shows the two single crystal surfaces of Ru. The Ru(0001) surface possesses the densest, i.e. hexagonal arrangement of atoms, **Fig. 1.1a**. The other plane, Ru(10 $\bar{1}$ 0), can have one of the two terminations of the surface atoms, **Fig. 1.1b**. One termination can be described as a stepped surface with a trigonal arrangement of atoms in two-atom-long terraces with a step of the same orientation; the other termination is a square-symmetrical arrangement of atoms in two-atom-long terraces with the same orientation of atoms in steps. In the faced-centered cubic (*fcc*) system, these three structures are uniquely defined and labeled as (111), (110), and (210), respectively.

---

<sup>\*</sup> present address: University of Delaware, Department of Chemical Engineering, Newark, DE 19716

## 2. Preparation of well-ordered Ru single-crystal surfaces

For over three decades, a procedure has been known for preparing well-ordered Ru single-crystal surfaces in ultra-high vacuum (UHV)<sup>4</sup>. It involves Ar<sup>+</sup> sputtering at room temperature, followed by several cycles of oxygen adsorption (at 800 K) and desorption (at 1700 K), both in an oxygen atmosphere of 10<sup>-7</sup> Torr; finally, the crystal is flash heated to 1700 K at UHV to remove traces of oxygen from the Ru surface. One of the first reports on voltammetry and *in situ* infrared (IR) spectroscopy of CO on the well-ordered Ru(0001) surface, appearing at the turn of the millennium, used this method for obtaining Ru(0001) single-crystal surfaces<sup>5</sup>. An easier method developed recently involved heating the Ru crystal in an H<sub>2</sub> stream<sup>6</sup>; it produced a well-ordered Ru(0001) surface as checked by Scanning Tunneling Microscopy (STM). This method shortened preparation time from days (UHV) to a few hours<sup>7,8,9</sup>. A modified method, subsequently reported further reduced the preparation time<sup>10</sup> in which crystals were inductively heated to 1700 K for 30-60 seconds in a stream of Ar-15% H<sub>2</sub>. STM pictures and voltammetry profiles on single-crystals thus obtained by were essentially the same as those from the other two methods.

## 3. Electrochemistry of single-crystal Ru surfaces

### 3.1. Voltammetry characterization

**Figure 3.1a** displays the voltammetry curves of polycrystalline and Ru(0001) surfaces in 1 M H<sub>2</sub>SO<sub>4</sub>. The broad, featureless oxidation-process at the polycrystalline electrode's surface involves currents about one order-of-magnitude larger than that of the single-crystal surface, and was attributed to the continuous oxidation of Ru in a process encompassing more than one electron per atom<sup>11,12,13</sup>. The potential regions of hydrogen adsorption and surface oxidation are generally acknowledged to almost overlap, since the Ru oxidation starts very early in the potential scale (0.2 V vs. RHE)<sup>1</sup>. The electrochemical processes are more easily identified for electrodeposited Ru films<sup>11,14,15</sup> than for bulk metal.

**Figure 3.1b** shows the voltammetry curves for the surface oxidation of Ru(0001) in 0.05 M H<sub>2</sub>SO<sub>4</sub>. Similar curves are presented in several publications<sup>5,9,16,17,18</sup>. Before starting a sweep in the positive direction, the potential was held sufficiently long at the negative limit to ensure a negligible reduction current originating from the previous potential cycle. The voltammetry curves show a single anodic peak with a long tail extending to the onset of bulk oxidation, and two major cathodic peaks correlated to the reduction processes, which begin at 0.6 V. Surface oxidation occurs above 0.4 V, and the integrated anodic charge reaches levels required for an one-electron oxidation of the Ru(0001) surface (260 μC cm<sup>-2</sup>) in the sweep up to 1 V. Increasing the sweep rate up to

---

<sup>1</sup> Unless otherwise stated, all potentials are expressed vs. reversible hydrogen electrode, RHE.

500 mV s<sup>-1</sup> caused a linear increase in the current density, but repeated potential cycling between 0 and 1.2 V did not significantly change the voltammetry curves. These facts suggest that the oxidation of the Ru(0001) surface is limited to the top layer with one electron per atom exchange at the potential below the onset of bulk oxidation. This can be represented by the following reaction,



Several groups have published voltammetry studies of the Ru(0001) surface in solutions containing non-specifically adsorbed ions<sup>5,8,9,16,17,18,19,20,21,22,23,24,25,26,27,28</sup>. The voltammetric profile of the Ru(0001) surface in 0.1 M HClO<sub>4</sub> has an integrated charge between 0.1 and 1 V of 230 μC cm<sup>-2</sup>, somewhat smaller than that required for an one-electron process, (dashed line in **Fig. 3.2a**). A comparison of the processes in the two electrolytes indicates an effect of anion adsorption on the oxidation of the Ru surface. Strongly adsorbed bisulfate anions prevent OH adsorption due to water-oxidation at low potentials, and promote the complete removal of the oxygen-containing species in the cathodic sweep. Comparing the electrochemical processes with the opening of the anodic limit in the two acid solutions suggests that the reduction process in perchloric acid solution cannot be completed without extending the sweep into the hydrogen adsorption/evolution region. Indeed, extending the cathodic limit into the H<sub>2</sub> evolution region generates a large peak around -0.05 V (full line in **Fig. 3.2a**). The peak's associated charge is over 300 μC cm<sup>-2</sup>, suggesting that it reflects a combination of at least two processes, one being hydrogen evolution. The other process, however, is puzzling. Since the same peak occurs in hydroxide solutions (see below), it is not due to perchlorate anion reduction. Also, it cannot be due to an impurity species in solution (like Cl<sup>-</sup>) because it is not supported with adequate voltammetry response. The probable explanation is the reduction of adsorbed OH, as also suggested in a recent publication<sup>29</sup>. The subsequent positive sweep shows a much greater peak around 0.2 V, and another, smaller one around 0.4 V. A total charge of over 600 μC cm<sup>-2</sup> is associated with the scan between -0.1 and 0.7 V.

To identify the nature of the species adsorbed at potentials from 0.1 to 0.25 V, a charge displacement technique was used that was shown useful in identifying species on the Pt(111) electrode<sup>30</sup>. The electrode potential was held at 0.12 V and CO was introduced into the cell; there was no significant CO oxidation on Ru(0001). The charge associated with the resulting displacement process was negative, adding up to -117 μC cm<sup>-2</sup> (see inset in **Fig. 3.2a**). If H<sub>ad</sub> was the adsorbed species in that potential region, the charge would be positive. Therefore, contrary the conclusions from other work, the reaction must be associated with some oxygen-containing species. This finding was confirmed recently using the same approach. A plausible reaction to account for this negative charge is



The measurement at 0.25 V revealed again a negative charge, albeit a smaller one, of  $-31 \mu\text{C cm}^{-2}$  implying that some transformation took place in the species existing at 0.12 V. The difference between the charges at 0.12 and 0.25 V is  $79 \mu\text{C cm}^{-2}$ , in good agreement with  $86 \mu\text{C cm}^{-2}$ , the voltammetric charge in that potential interval. Interestingly, measurements in  $\text{H}_2\text{SO}_4$  solution do not show this process; it is probably precluded by strong bisulfate adsorption on the hexagonal structure of Ru(0001). As discussed later in this chapter, infrared spectroscopy and X-ray diffraction studies indicate that bisulfate adsorption on Ru(0001) is essentially at saturation coverage between 0.0 and 0.5 V, and that water chemisorbs on Ru(0001) in the absence of chemisorbed anions<sup>16,17</sup>.

Anion effects on the electrooxidation of Ru(0001) were explored by introducing  $\text{Cl}^-$  and  $\text{Br}^-$  into the 0.1 M  $\text{HClO}_4$  solution. A sharp rise of anodic current occurs near 0.2 V, which is at a more negative potential than the onset of surface oxidation in sulfuric acid. Hence, even though halide ions are strongly adsorbed, they do not better protect the Ru from surface oxidation than do bisulfate ions. It is likely that a different redox process occurs with halide ions because they form compounds with Ru in several different oxidation states.

Voltammetry of the oxidation of Ru(0001) in 0.1 M NaOH, **Fig. 3.2b**, shows a curve that has some similarities to that recorded in perchloric acid. The curve is dominated by a strong anodic peak at 0.25 V and a strong cathodic peak occurring at -0.05 V, the same potential as in perchloric acid. Its origin is not understood, as discussed. The multitude of peaks indicates the complexity of the oxidation/reduction processes. The symmetric peaks in this potential range on polycrystalline Ru were attributed to processes involving hydrogen adsorption and/or Ru oxidation<sup>13,31,32</sup>.

The voltammetry curve for the Ru(10 $\bar{1}$ 0) surface in 0.05 M  $\text{H}_2\text{SO}_4$  solution (**Fig. 3.3a**) reveals a remarkable difference between the oxidation processes for Ru(0001) and Ru(10 $\bar{1}$ 0). The oxidation of this face is more facile than that of Ru(0001), as indicated by the onset of the reaction at lower potentials and by increase of the charge with each potential cycle. This difference most likely is the consequence of the more open structure of the Ru(10 $\bar{1}$ 0). A pair of peaks at 0.12 and 0.3 V is reminiscent of hydrogen adsorption on Pt metals. However, CO displacement showed a negative charge of  $-354 \mu\text{C cm}^{-2}$ . Thus, the peaks probably represent partial Ru oxidation to RuOH, wherein OH is the predominant adsorbed species, perhaps with some co-adsorption of bisulfate.

Unlike the behavior of the Ru(0001) surface, the gradual increase in the positive potential limit has deleterious effects on the ordering of Ru(10 $\bar{1}$ 0). The increase of the charge associated with the voltammetry curve in each subsequent cycle indicates the oxidation of several of the crystal's top atomic layers, similar to the behavior of polycrystalline Ru<sup>11,12,13</sup>.

**Figure 3.3b** shows the cyclic voltammetry of the Ru(10 $\bar{1}$ 0) surface in 0.1 M  $\text{HClO}_4$ . The voltammetry profile differs from that in sulfuric acid solution suggesting that sulfate absorption/desorption contributes to the peaks observed in **Fig. 3.3a**. The total

charge in the positive sweep between 0 and 0.25 V is  $247 \mu\text{C cm}^{-2}$ , which is greater than that required for an one-electron oxidation ( $159 \mu\text{C cm}^{-2}$ ). The process that occurs between 0.05 and 0.3 V is probably associated with a large uptake of  $\text{OH}_{\text{ad}}$ . Potential cycling to 0.8 V causes additional growth of oxide on this surface (cf. **Fig. 3.3a**), unlike the behavior of the Ru(0001) face. The striking differences between the two Ru single-crystal planes reveals the large stability of the hexagonal Ru(0001) surface and a pronounced reactivity of the rectangular Ru( $10\bar{1}0$ ) face.

### 3.2 Surface X-ray diffraction study

The electrochemical surface oxidation of Ru(0001) was characterized by *in situ* surface X-ray scattering techniques in acid solutions at potentials where the voltammetry curves show an one-electron surface oxidation process below the onset of bulk oxidation. The analysis of the X-ray specular reflectivity found that the spacing between the top two Ru layers is 0.213 nm at 0.1 V, and 0.220 nm at 1.0 V in 1 M  $\text{H}_2\text{SO}_4$  solution, similar to those in the gas phase for bare Ru and for one monolayer (ML) of oxygen on Ru (0.210 and 0.222 nm, respectively). At low potentials, the specular reflectivity data support a model involving the co-adsorption of bisulfate and hydronium ions on Ru(0001). The coverage of bisulfate is close to 1/3 ML at potentials below 0.57 V. **Figure 3.4** shows the proposed structural models. In contrast to the behavior of Pt(111) and Au(111) surfaces, no place exchange is involved in Ru(0001) surface oxidation. The formation of a monolayer of ruthenium oxide induces partial desorption of bisulfate, in agreement with the Fourier Transform infrared (FTIR) results (see **section 3.3**). Strikingly, oxygen penetration is completely blocked on Ru(0001) at potentials below the bulk oxidation potential, in contrast to the high degree of surface oxidation of polycrystalline Ru that occurs between the onset of hydrogen evolution to the onset of bulk oxidation. Since gas-phase studies demonstrated that subsurface oxygen plays a major role in the activity of Ru for CO oxidation, the lack of subsurface oxygen on the Ru(0001) electrode might explain its inactivity for CO electrooxidation; this interpretation is discussed below.

### 3.3. Infrared spectroscopy and anion adsorption

The adsorption of anions on solid surfaces is of considerable interest, mainly because of its effect on the kinetics of electrochemical reactions. Several *in-situ* techniques have been applied toward this purpose<sup>33</sup>. Infrared measurements were used to identify adsorbed species, estimate anion adsorption isotherms, and to gain information on anion interaction with electrode surfaces<sup>34</sup>. Sulfuric acid anions are possibly the commonest anion adsorbates because of their specific adsorption on metal surfaces. Depending on the metal, its surface orientation, and the concentration of anion, either sulfate or bisulfate can be specifically adsorbed on the surface. Identifying the

predominant adsorbate on platinum-group metals has engendered some controversy. While STM studies show that sulfate and/or bisulfate on Pt metals of (111) orientation form a ( $\sqrt{3} \times \sqrt{7}$ ) overlayer<sup>35</sup>, questions remain about the nature of the species. Even though the symmetry differences of sulfate and bisulfate ions should, in principle, reveal the preferentially adsorbed species, the interpretation of the mostly equivalent *in situ* IR spectra may not be unique<sup>36</sup>. Two absorption bands around 1200 and 1100  $\text{cm}^{-1}$  observed on a polycrystalline Pt electrode were attributed to adsorbed bisulfate and sulfate, respectively<sup>37</sup>. In addition, a third band at 950  $\text{cm}^{-1}$  on polycrystalline Pt, led to the conclusion that both bisulfate and sulfate on the surface give rise to three bands<sup>38</sup>. For Pt (111), Nart et al. concluded that the adsorbate is sulfate coordinated via three oxygens presenting a  $C_{3v}$  symmetry, while Faguy et al. argued that the adsorbed species is not described adequately as either sulfate or bisulfate but rather as an  $\text{H}_3\text{O}^+ - \text{SO}_4^{2-}$  ion pair<sup>39</sup>.

Recent data confirmed that the preferred species on Pt (111)<sup>40</sup>, Pd<sup>41</sup> and Ir<sup>42</sup> is bisulfate, while sulfate adsorbs on Ag(111)<sup>43</sup> and on Au(111)<sup>44,45,46</sup>. Apparently the *sd* metals (Rh, Pt, Pd) with (111) orientation adsorb bisulfate, whereas the *sp* metals (Cu, Ag, Au) adsorb sulfate. The IR study on Ru(0001) seemed to support this conclusion (see below), as the latter has the same orientation of surface atoms as the *fcc* metals of (111) orientation, and the adsorbed species is bisulfate.

### 3.3.1. Polycrystalline Ru electrode

As discussed in the previous sections, electrochemical oxidation of polycrystalline Ru involves about one order-of-magnitude larger currents than that of Ru(0001), starting as early as 0.2 V. Polycrystalline Ru is covered with hydroxyl ions from water very early in the potential scale even in acidic solutions, thus blocking the surface from anion adsorption by the supporting electrolyte. This conclusion is supported by the *in situ* IR spectra presented below.

Specific adsorption of sulfate-bisulfate generally displays spectral features that are blue shifted (i.e., to higher frequencies) with higher electrode potentials, as observed for both polycrystalline Pt<sup>37,38,47</sup> and the Pt(111) surface. The shift is explained in terms of one or more of the following mechanisms: electron donation between the adsorbate and the metal surface (vibronic coupling); coupling of the electric field that exists in the double layer with the dipole moment of the adsorbates (Stark effect); and, the interaction from dipole–dipole coupling due to an increase in coverage<sup>48,49</sup>. The absence of these mechanisms in the IR spectra shown in **Fig. 3.5a** for polycrystalline Ru –  $\text{H}_2\text{SO}_4$  system suggests that there is no specific adsorption of sulfuric acid anions.

Five distinctive, potential independent peaks are observed at 1100, 980, 1205, 1051, and 885  $\text{cm}^{-1}$  from the polycrystalline Ru surface in 0.05 M  $\text{H}_2\text{SO}_4$  (see **Fig. 3.5a**). The spectra have peaks. The first two are associated with sulfate and the rest with the bisulfate species<sup>50</sup>. Positive-going bands in the  $-\Delta R/R$  representation show an increase of the species at the electrode's surface and/or in the solution layer sampled by the IR light at the sample's potential relative to that at the reference potential. However, adsorbed

species at the electrode surface are sensitive only to the *p*-polarized light due to the surface-selection rule, while both polarizations interact equally with randomly oriented species in solution<sup>51</sup>. The fact that the intensity of both the sulfate and bisulfate bands rises with increasing electrode potential, and that their features are observed with both *s*- and *p*-polarized light, suggests strongly that the spectra represent solution species, i.e., the migration of ions into the diffuse part of the double layer to compensate for the charge buildup at the electrode surface. Therefore, a marked interaction of OH with polycrystalline Ru electrode at low potentials prevents sulfate-bisulfate adsorption throughout the whole potential region from hydrogen evolution to oxygen evolution.

### 3.3.2. Ru(0001) and Ru(10 $\bar{1}$ 0) single-crystal electrode surfaces

**Figure 3.5b** shows a set of spectra taken at the Ru(0001) electrode in 0.05 M H<sub>2</sub>SO<sub>4</sub> solution. There is a well-defined bipolar peak with the positive lobe centered at 1280 cm<sup>-1</sup> that shifts with increasing potential. A similar band has been observed for several single crystal surfaces with hexagonal surface orientation<sup>52</sup>. On the basis of *ab initio* calculations for anion adsorption at the Pt(111) surface, Sawatari et al. concluded that the totally symmetric stretch of bisulfate at 1051 cm<sup>-1</sup> should undergo a large frequency shift<sup>53</sup>. In the IR spectrum given in the  $-\Delta R/R$  representation, this phenomenon should be visible as a positive-going, potential-dependent peak around 1250 cm<sup>-1</sup>, together with a negative-going 1051 cm<sup>-1</sup> band representing the loss of HSO<sub>4</sub><sup>-</sup> species in solution. The two bands were observed in the Pt(111) / H<sub>2</sub>SO<sub>4</sub> system, and the strongly blue-shifted band was assigned to the absorption of the bisulfate or sulfate-hydronium ion pair. Consequently, the band at 1280 cm<sup>-1</sup> in the present case arises from bisulfate adsorption at Ru(0001). However, the bipolarity of the peak is unusual, as it has not been noted in any other sulfate-bisulfate adsorption studies<sup>39,43,52</sup>. Furthermore, the peak for bisulfate ions in solution is visible only above 0.45 V. Both phenomena appear to be related to the bisulfate adsorption at the reference potential. The absence of the solution band at 1051 cm<sup>-1</sup> at potentials below 0.45 V indicates the lack of a measurable change in the bisulfate coverage at the sample and reference potentials, i.e., that a sizeable coverage of bisulfate is attained already at the reference potential of 0.03 V. This conclusion is supported by the bipolar shape of the band for adsorbed bisulfate at 1280 cm<sup>-1</sup> because such a band in subtractive normalized interfacial FTIR (SNIFTIR) spectra is apparent when a species is absorbed at both the reference and sample potential, and the frequency of its band center depends upon potential<sup>54</sup>.

**Figure 3.5b** also reveals that the positive lobe of the bipolar band around 1280 cm<sup>-1</sup> decreases at potentials above 0.45 V; this decline coincides with the onset of the surface oxidation in the voltammetry of Ru(0001) (c.f. **Fig. 3.1**). Adsorption of the OH species is followed by the desorption of bisulfate and a concurrent increase in the bisulfate species in the double layer. This effect becomes visible in the IR spectrum by the appearance of the positive-going solution-phase bands for the bisulfate anion at 1051 and 1200 cm<sup>-1</sup> at potentials equal to, or higher than 0.55 V. The most pronounced feature in the IR spectra

above 0.55 V is the negative lobe of the bipolar band centered at  $1248\text{ cm}^{-1}$ , which represents adsorbed bisulfate at the reference potential.

The open structure of the Ru(10 $\bar{1}$ 0) surface (c.f. **Fig. 1.1b**) is expected to react with H<sub>2</sub>O at very low potentials and become covered with OH species. UHV data indicate that oxygen adsorption on this surface produces c(2x4)-2O and (2x1)p2mg-2O overlayers with O atoms occupying the three-fold *hcp* sites formed by two atoms in the first atomic layer and one atom in the second layer<sup>55</sup>. These three-fold sites are the only likely candidates for sulfate or bisulfate adsorption on either of the two terminations of the Ru(10 $\bar{1}$ 0) surface. Since the latter are occupied, it is not surprising that this plane shows no sulfate or bisulfate adsorption in IR spectra (not shown). The surface remains inactive for anion adsorption even after extensive hydrogen evolution, which was shown to free some oxygen-occupied sites in the first atomic layer<sup>7</sup>.

### 3.4. Surface-oxide formation

The specific catalytic properties of polycrystalline and single crystal surfaces have prompted extensive research on their oxidation in electrochemical- and gas- phase environments<sup>17,55,56</sup>. Recent developments in fuel cell technology have renewed efforts to improve Pt-Ru electrocatalysis for both reformate hydrogen- and methanol-oxidation<sup>57</sup>. In the following section, we discuss the oxidation of single crystal surfaces in both UHV- and electrochemical- environments.

#### 3.4.1. Gas-phase oxidation

In general, the catalytic activity of transition metal surfaces for certain oxidation reactions (*e.g.* CO) is determined by the propensity of the metal's surface to dissociate oxygen molecules and is counterbalanced by the bond strength of the active oxygen species on the metal's surface<sup>58</sup>. The transition metals with half-filled *d*-bands reveal the highest activity, where the dissociation probability is not too low and the adsorption energy is not too high. Accordingly, Pt, Pd, and Rh are efficient metal catalysts, while Ru is a poor one due to its very high oxygen-binding energy.

On the other hand, UHV measurements showed that the Ru surface can be used as a kind of storage, able to accommodate large amounts of atomic oxygen<sup>59,60</sup>. Other transition metals also exhibit this ability, but the exceptional property of Ru surfaces is due to the fact that oxygen can be completely removed by simply heating the sample up to about 1700 K without irreversibly incorporating oxide in the bulk. The oxidation of the Ru(0001) surface in UHV at low O<sub>2</sub> pressure facilitates the formation of (2 x 2)-O and (2 x 1)-O superstructures at coverages of 0.25 and 0.5 ML, respectively. Both superstructures have minimal catalytic activity for CO oxidation. Even the (1 x 1)-O overlayer on Ru(0001), prepared at elevated temperatures by the enrichment of the (2 x

1)-O phase due to the decomposition of  $\text{NO}_2$ <sup>61</sup> is inactive a catalyst. The high reactivity of the Ru(0001) surface for CO oxidation is only reached when the total  $\text{O}_2$  concentration exceeds the equivalent of about 3 ML, *i.e.*, when at least 2 ML of oxygen are located in the subsurface region and the reaction probability increases by two orders-of-magnitude<sup>62,63</sup>. The active part of this “O-rich” ruthenium phase, prepared by directly exposing the Ru(0001) surface to high doses of  $\text{O}_2$  at elevated temperatures, was demonstrated to be  $\text{RuO}_2$ , growing epitaxially with its (110) plane parallel to the Ru(0001) surface<sup>64</sup>. Its extraordinary activity towards CO oxidation was reported in several papers<sup>65</sup>.

Similar growth of  $\text{RuO}_2(110)$  on Ru(0001) can be achieved by annealing the substrate in Ar containing *ca.* 100 ppm of  $\text{O}_2$  at around 700 K. The epitaxial growth of  $\text{RuO}_2$  at elevated temperatures on Ru(10 $\bar{1}$ 0) was demonstrated with its (100) face oriented parallel to the substrate. An electrochemical STM image (ECSTM) of  $\text{RuO}_2$  prepared by chemical oxidation of Ru(0001) in Ar/ $\text{O}_2$  (115 ppm), obtained in 0.05 M  $\text{H}_2\text{SO}_4$  under an open-circuit potential shows stripes with step sizes of about 0.3 nm (*i.e.*, corresponding to one monolayer of oxide) growing unidirectionally at  $60^\circ$  with respect to the steps' direction, **Fig. 3.6a**. An atomically resolved ECSTM image from the stripes, **Fig. 3.6b**, reveals a rectangular unit cell that agrees well with the ideal rutile structure of  $\text{RuO}_2$  with an (110) orientation<sup>66</sup>. The model of ideal the  $\text{RuO}_2(110)$  single-crystal surface is depicted in **Fig. 3.7**. LEED and STM data for UHV oxidation of Ru(0001) suggest that  $\text{RuO}_2$  overlayer is not pseudomorphic with the Ru substrate<sup>64,67</sup>. Between the  $\text{RuO}_2$  domains, the Ru surface is covered with a monolayer of RuOH, which is the precursor to Ru oxidation.

### 3.4.2. Electrochemical oxidation

The initial phase of the electrochemical oxidation of Ru(0001) in 0.05 M  $\text{H}_2\text{SO}_4$  is a hump at *ca.* 0.57 V (*c.f.* **Fig 3.1**). At lower potentials the surface is protected by bisulfate adlayer<sup>16,17</sup>. **Figure 3.8** shows ECSTM images obtained by progressively increasing the electrode's potential.

At 1.0 V, **Fig. 3.8a**, the Fourier transform of an atomically resolved ECSTM image obtained from a terrace reveals a hexagonal array of dark spots at distances of 0.270 nm, corresponding to the inter-atomic distance of the Ru atoms. The dark contrast of the spots suggest that they are associated with RuOH, as shown in the UHV studies of chemisorbed O atoms in the (1 x 1) overlayer on the Ru(0001) surface<sup>23,64</sup>. Identical large-frame images are obtained at any potential between 0.05 and about 1.10 V. The first observable changes, which appear as a difference in contrast at the step edges, occur at a potential of 1.17 V, indicating their coverage by oxide (**Fig 3.8b**). The steps' edges are covered with irregularly spaced oxide islands separated by non-oxidized segments. At the onset of bulk oxidation, ECSTM image shown in **Fig. 3.8c** reveals smooth RuOH domains, oxide islands along meandering step edges, and large oxide islands concentrated mainly near the steps' edges. The latter suggests that the Ru atoms

necessary for oxide growth come from the dissolution of the step edges, rather than terraces. The same type of topographical features is observed at 1.35 V (**Fig. 3.8d**) but with more large oxide- islands, twisting step-edges, and smaller area of smooth RuOH domains. The dimensions of the large oxide islands are the same as in **Fig. 3.8c**, indicating that they do not grow with increasing potential; rather, only their number increases. These randomly distributed islands represent RuO<sub>2</sub> domains, in accordance to the Pourbaix diagrams<sup>68</sup> and an *ex situ* study of Ru(0001) oxidation in a similar potential region; their nucleation process is instantaneous, as verified by potential step experiments.

## 4. Electrocatalysis on Ru single-crystals and nanoparticle surfaces

The ruthenium surface shows certain activity in hydrogen evolution, oxygen reduction, and CO oxidation; it is not active for methanol oxidation because methanol is not adsorbed on oxygen-covered Ru. The unique activity of Pt-Ru catalysts towards methanol is briefly discussed in **section 5**.

### 4. 1. Hydrogen oxidation and evolution reactions

While it is expected that electrocatalytic reactions on Ru surfaces should be strongly structure-sensitive, the first report on structural effects on hydrogen oxidation and evolution reactions appeared only recently. The structural effects in the hydrogen oxidation reaction (HOR) and the hydrogen evolution reaction (HER) may be factors affecting the performance of hydrogen fuel cell anodes.

Hydrogen oxidation on Ru is likely to proceed through a mechanism involving two or three of the following reactions, as on Pt<sup>69,70</sup>:



For the hydrogen-evolution reaction, these processes are referred to as the recombination reaction, or Tafel reaction, the ion-plus-atom reaction, or Heyrovski reaction, and the charge transfer reaction, or Volmer reaction, respectively. As mentioned above, there are disagreements about the existence of underpotential deposition of hydrogen at Ru surfaces<sup>18,23</sup>. If the peaks preceding the hydrogen evolution at Ru single crystal surfaces were due to the adsorption / desorption of OH, as the above discussion indicates, then a rate expression for the hydrogen-oxidation reaction would have to include the coverage of both adsorbed species, i.e.,  $\theta_{\text{OH}}$  and  $\theta_{\text{H}}$ , and it would be difficult to obtain an indication of the rate-determining step of these three reaction processes from the Tafel slopes.

The kinetics of the HOR on polycrystalline Ru and carbon-supported nanoparticles is about two orders-of-magnitude smaller than that on Pt or Pt-Ru alloys, and it usually is assumed that the Ru contribution to the H<sub>2</sub> oxidation current of fuel cell anodes is negligible<sup>71,72</sup>. However, at temperatures at which PEMFCs operate (60 – 80 °C) the kinetics of HOR on Ru is considerably faster than at room temperature, so that the effect of Ru surfaces may be of importance in PEMFC catalysis.

The hydrogen oxidation reaction was found to be under kinetic control at both Ru(0001) and Ru(10 $\bar{1}$ 0) surfaces. Dependence on the rotation rate is negligible on the (0001) surface, while that on (10 $\bar{1}$ 0) is significant, but the limiting current density is not linear with the square root of the rotation rate. On the more open Ru(10 $\bar{1}$ 0) surface, the peak current densities are about twice as large than those on hexagonal Ru(0001) surfaces at room temperature, as well as at higher temperatures in 0.05 M H<sub>2</sub>SO<sub>4</sub>, **Fig. 4.1**. On both surfaces the reaction rate rapidly falls with increasing overpotentials, causing almost complete inhibition at potentials above 0.6 V, due to the growing oxide layer<sup>73</sup>. Purportedly, hydrogen can still be adsorbed on the ridges of (10 $\bar{1}$ 0) surface despite the early coverage by oxygen-containing particles, while the latter causes complete inhibition on the smooth Ru(0001) surface. In perchlorate solutions, the more open (10 $\bar{1}$ 0) surface again exhibits higher currents for H<sub>2</sub> oxidation, but considerably lower than those in sulfuric acid solution. As perchlorate ions are not considered to be specifically adsorbed on metal surfaces, the lower kinetics in HClO<sub>4</sub> is probably due to the larger oxide build-up at low potentials.

The apparent electrochemical-activation energy for the HOR,  $\Delta H^{0\#}$ , on the Ru(0001) is about tenfold higher than on the Pt surface with identical atomic arrangement, Pt(111). Similarly,  $\Delta H^{0\#}$ , on the Ru(10 $\bar{1}$ 0) surface is about one order-of-magnitude higher than that on Pt(110), in agreement with the large difference in the observed reaction rates on Ru and Pt<sup>72, 73</sup>.

The structural effects on hydrogen evolution kinetics on Ru are small, as inferred from the HER curves for (0001)- and (10 $\bar{1}$ 0)-oriented surfaces obtained in perchloric and sulfuric acid solutions<sup>7</sup>. The similarities in the reaction kinetics in the two indicate that hydrogen evolution proceeds on bare Ru surface, i.e., a surface not covered with either OH or, in the case of sulfuric-acid solutions, with bisulfate ions.

## 4. 2. CO oxidation

Carbon monoxide is one of the best characterized adsorbates in catalysis because of its specific role in many catalytic reactions. Since it is a strongly adsorbed species, it usually blocks the catalyst's surface for desired reactions, for instance in the oxidation of methanol or hydrogen reformat.

Gas-phase oxidation of CO on the Ru surface has been the topic of numerous investigations<sup>6,61, 74, 75, 76, 77</sup>. While bare Ru(0001) surfaces and those with up to a monolayer coverage with oxygen have low reactivity, oxygen coverages above 3 ML

play a role in the high reactivity of Ru(0001). The efficiency was proposed to arise from the subsurface oxygen layer, with an integral reaction yield about two orders-of-magnitude higher than for samples with an adsorbed oxygen layer only<sup>62,78</sup>. Two explanations are offered for the catalytic enhancements that include modification of the structure and the electronic properties by the oxygen dissolved or incorporated in the Ru surface. In the first model, the redistribution of electron density in the topmost Ru layer induced by subsurface oxygen lowers the activation barrier for the reaction with CO. The second concept postulated that the subsurface-oxygen phase consists of mobile oxygen atoms that can participate in CO oxidation only via thermal diffusion after reaching the topmost surface layer, the latter process being the rate-limiting step in CO oxidation. In either case, it was argued that a surface containing a large amount of oxygen in the subsurface region provides new adsorption sites for oxygen at the topmost surface layer, thereby creating a new oxygen phase, and raising by tenfold the probability for CO/CO<sub>2</sub> conversion at room temperature<sup>79</sup>. Such kind of oxygen bond does not exist at a bare Ru surface. The existence of this oxygen-rich phase was disputed recently, and the high CO-oxidation activity attributed to a RuO<sub>2</sub>(110) film epitaxially grown on Ru(0001). This interpretation is more or less generally accepted today.

In the electrochemical environment, the oxidation of pre-adsorbed CO is known to proceed through a two-step (Langmuir-Hinshelwood) mechanism<sup>80</sup>. The first step involves the adsorption of OH, while, in the second step, the adsorbed OH causes oxidation of CO:



where \* denotes an empty site on the metal. On Pt, the rate-determining step is the first reaction, as electro-oxidation starts as soon as OH adsorption sets in. However, the second step appears to be the rate-determining one on Ru, as the metal's surface is covered with OH<sub>ad</sub> very early in the potential scale, before the onset of oxidation (*vide supra*).

The first demonstration of electrochemical oxidation of CO on Ru(0001) by cyclic voltammetry and SNIFTIRS was made only recently. Simultaneously, a first observation was reported of CO adsorption using FTIR and STM. Unlike the polycrystalline Ru surface where only on-top linearly bonded CO (CO<sub>L</sub>) is visible<sup>5,81</sup>, CO adsorption on Ru(0001) shows contributions from both CO<sub>L</sub> and multiple-bonded CO (CO<sub>H</sub>)<sup>5,6</sup>. While a certain amount of activity towards CO oxidation to CO<sub>2</sub> was seen on the surface of polycrystalline Ru, Ru(0001) exhibited almost none, judged by the absence of the FTIR peak<sup>5</sup> around 2350 cm<sup>-1</sup>. At low CO doses, the STM image showed a (√3 × √3) R 30° CO overlayer with a coverage of 0.33 ML, similar to the structures found with UHV; a further increase in CO doses produced a new c(2 × 2)-2CO structure as the saturation phase, where CO occupied both the on-top and the three-fold hollow sites, with coverage of 0.5 ML. A combined electrochemical, STM and FTIR study of CO on bare and Pt-

modified Ru(0001) and Ru(10 $\bar{1}$ 0) surfaces followed<sup>82</sup>.

This study revealed that the electrochemical oxidation of CO at the Ru(0001) surface occurs at negligible rates, probably only at surface imperfections. **Figure 4.2** shows STM image of the Ru(0001) surface after slight mechanical polishing with 0.05  $\mu\text{m}$  alumina slurry, starting from a well-ordered one, shown in **Fig. 3.7a**. A comparison of **Figs. 4.2** and **3.7a** reveals that the mechanical polishing results in significant reduction of terrace widths and introduction of kinks in step edges. Interestingly, this surface shows voltammetry curve almost identical to the one obtained with well-prepared crystal<sup>83</sup>. Apparently, the cyclic voltammetry is insensitive to the surface imperfections in Ru(0001). This can be explained if Ru atoms in edges and kinks are more extensively oxidized than those in terraces. Since such Ru atoms cannot be easily reduced, thus they do not contribute to the charge in voltammetry and behave as passivated surface. This assumption seems quite plausible because the surface depicted in **Fig. 3.8b**, having highly oxidized steps, shows a similar voltammetry curve as the surface presented in **Fig. 3.8a**. We speculate that this oxide reacts with CO in the same manner as RuO<sub>2</sub> does it in gas phase. Thus, it appears that strongly oxidized steps are the cause for the observed activity of mechanically polished Ru(0001) for CO oxidation (see below).

The cyclic voltammetry of CO oxidation on two Ru single crystal surfaces is presented **Fig. 4.3**. The more open structure of Ru(10 $\bar{1}$ 0) has a sizeable activity, several times larger than that of Ru(0001). Interestingly, it is also larger than that of the polycrystalline Ru in the positive scan (not shown). **Fig. 4.3** shows that a well ordered Ru(0001) is very inactive for CO oxidation. Introduction of steps enhances oxidation, as observed by Jin et al.<sup>84</sup> and confirmed by Lee et al.. No oxidation is apparent on Ru(10 $\bar{1}$ 0) in the CO-saturated solution in the negative scan if the upper limit is above 0.8 V, as confirmed by progressively opening the upper limit. This phenomenon, also observed at polycrystalline Ru electrodes, could be related to either too high a surface oxide-coverage at the electrode's surface, or to the different oxidation state of Ru at these potentials. Furthermore, the adsorption rate of CO on an oxide-covered surface produced at high potentials probably differs from that at the RuOH-covered surface at low potentials.

The surface imperfections in Ru(0001) from mechanical polishing appear responsible for a sizable activity of CO oxidation that resulted in the spectra with peaks around 2346, 2010 and 1780  $\text{cm}^{-1}$ . They correspond to CO<sub>2</sub> in solution, CO<sub>L</sub> and CO<sub>H</sub>, respectively **Fig.4.4**. Interestingly, in the FTIR spectra for the oxidation of CO on a Ru(10 $\bar{1}$ 0) single crystal electrode, **Fig. 4.5**, the CO<sub>H</sub> is not observed. While the three-fold hollow sites can be found on a well-ordered Ru(10 $\bar{1}$ 0) surface (*c.f.* **Fig. 1.1b**), the steric effects of the energetically favored CO<sub>L</sub> probably prevent their adsorption of CO. The CO adsorption tuning rates ( $\Delta\nu(\text{CO}_L) / \Delta E$ ) on both single crystal surfaces is lower than that on any platinum-group metal. The tuning rate of 20 and 26  $\text{cm}^{-1} \text{V}^{-1}$  for Ru(10 $\bar{1}$ 0) and Ru(0001) surfaces, respectively, may be correlated in the former to the presence of the oxide at all potentials, or to the high coverage of CO at both on-top and three-fold hollow sites in the latter case.

### 4. 3. Oxygen reduction reaction

Electrocatalytic oxygen reduction reaction (ORR) is of a great importance to electrochemical energy conversion in fuel cells and metal-air batteries, and plays a major role in corrosion. The slow reaction kinetics of the ORR decreases the fuel cell's efficiency. The major problem is the large potential deficiency during the initial portion of the polarization curve, partly attributed to the inhibition of OH adsorption on Pt at very positive potentials. On a polycrystalline Ru in alkaline and acid media, the ORR proceeds through a 'parallel' mechanism, wherein the kinetics strongly depends on the thickness of the oxide layer in the former, and a predominant 'series' pathway with the exchange of approximately four electrons in the latter solution<sup>13,31</sup>. No catalytic decomposition of O<sub>2</sub> and HO<sub>2</sub><sup>-</sup> species occurs, and the rate constants for these two species reactions were determined. Tafel slopes indicated that the first charge transfer was the rate-determining step<sup>13,31</sup>.

To establish the structural sensitivity of the ORR, single crystal surfaces were used. **Figure 4.6** shows ORR on a rotating Ru(10 $\bar{1}$ 0) electrode as a function of the potential and rotation rate. The reaction appears to be under mixed kinetic and diffusion control over a wide potential range. At the most negative potentials, the ring current decreases to a negligible value, suggesting a complete four-electron reduction of O<sub>2</sub> in that region. The Tafel slope obtained was -128 mV per decade, surprisingly close to the expected value of -120 mV per decade for the slow, first charge-transfer step, even though the Ru surface is covered with OH. The number of electrons,  $n$ , exchanged per reduced O<sub>2</sub> molecule was calculated assuming first-order kinetics for the dissolved O<sub>2</sub>. The experimental value of the slope obtained from a Koutecky-Levich plot agrees with the calculated value for  $n=4$ . A small dependence of  $n$  on potential is related to the generation of small amount of H<sub>2</sub>O<sub>2</sub>.

Oxygen reduction on Ru(0001) (not shown) appears to be under considerable kinetic control. A diffusion-limiting current is not reached until the potential of hydrogen evolution, as seen for polycrystalline Ru in acid solutions. Unlike the behavior of Ru(10 $\bar{1}$ 0), sweeps in anodic direction almost retrace the curves in cathodic sweeps, suggesting that the behavior of the surface processes are reversible under these conditions. A Tafel slope of -135 mV per decade was obtained for 1600 rpm. The limiting current for Ru(10 $\bar{1}$ 0) is not reached before the most negative potentials, and is taken for  $j_d$ . A slope larger than -120 mV points to an additional drop in voltage at the oxide layer, which is a plausible explanation for the reaction on the Ru(0001) surface covered by a monolayer of RuOH. Therefore, the observed slope is an indication of the slow, first charge-transfer rate determining step, as in the case of Ru(10 $\bar{1}$ 0).

## 5. Pt-Ru fuel cell electrocatalysts

Reviewing the work on the Pt-Ru electrocatalysts is beyond the scope of this article. We will briefly comment on some key advances in this area. Although early

discovery by Petrii<sup>85</sup>, and Bockris and Wroblowa<sup>86</sup> established the catalytic activity of Pt-Ru alloys for methanol oxidation, despite of active investigation, even the optimum composition of Pt–Ru is yet to be firmly settled. An early explanation for the mechanism by which bimetallic catalysts improve upon the performance of pure Pt, that is, the bifunctional mechanism proposed by Watanabe and Motoo<sup>87</sup>, was recently challenged.

The bifunctional mechanism is explained in terms of the independent function of atoms of different metals: methanol adsorption and decomposition takes place on Pt, while the alternative metal atoms provide preferred sites to bind OH. Several metals, such as Ru, Sn and Mo<sup>88, 89, 90</sup>, were assessed in combination with Pt. Recent works in developing fuel cell technology have renewed the efforts to improve Pt-Ru electrocatalysts for reformate hydrogen- and methanol-oxidation, in which Ru provides active oxygen for oxidizing strongly bound CO on Pt. It was noted that the atoms substituted for Pt alter the surface electronic structure. Accumulated evidence suggests that substitution changes the binding energy of adsorbates, and so the bifunctional mechanism should be altered to reflect changes in the adsorption bond. Krausa and Vielstich examined the oxidation of small molecules on Pt and a Pt–Ru alloy by differential electrochemical mass spectrometry (DEMS), and noted a cooperative effect on the alloy's electrode, which they interpreted as evidence of a modification in the Pt electronic structure<sup>91</sup>. McBreen and Mukerjee recorded a decrease in Pt-Pt bond length in X-ray absorption studies of Pt–Ru electrode surfaces that they correlated with an increase in *d*-band vacancies<sup>92</sup>. They concluded that the bifunctional mechanism needs to be modified to account for a cooperative electronic effect in the Pt–Ru catalyst. On the other hand, Gasteiger et al. argued that the binding energy of CO to pure Ru under UHV is not different enough from the binding energy on pure Pt to mandate such alterations.

## 5.1. Pt submonolayers on Ru single-crystal surfaces

Existing fuel cell technology suffers from at least two problems. One is the low CO tolerance of anodes for the oxidation of reformate hydrogen, impure hydrogen, or methanol. Small concentrations of CO are inevitable in H<sub>2</sub> produced by reforming methanol or other hydrocarbons, and the performance of Pt-based catalysts is strongly impaired by the presence of small amounts of CO. The other problem is the high Pt loading, which is the major constituent of Pt-Ru catalysts.

Adzic and coworkers proposed a radically new approach in electrocatalysis and catalysis<sup>93</sup> that can alleviate both problems. It is based on a catalyst consisting of only a submonolayer Pt deposited on carbon-supported Ru nanoparticles. The Pt submonolayer on Ru (PtRu<sub>20</sub>) electrocatalyst demonstrated higher CO tolerance than commercial catalysts in rotating disk experiments. Tests of the long-term stability of the fuel cells detected no loss in performance over 870 h, even though the Pt loading was approximately 1/10 of the standard loading. *In situ* X-ray adsorption spectra (XAS) indicated an increase in the *d*-band vacancy of deposited Pt, which may facilitate partly

the reduced susceptibility to CO poisoning for this catalyst. Below, we describe the single crystal experiments leading to the new catalyst, the synthesis of high-surface-area catalyst, and its characterization and performance.

The synthesis of the PtRu<sub>20</sub> was facilitated by the discovery of electroless (spontaneous) deposition of Pt on Ru, which was not observed for noble-metal substrates. In the electroless deposition of Pt on an Ru(0001) single crystal surface<sup>94</sup> the surface morphology, and the amount and the uniformity of the Pt deposited can be varied by changing the concentration of [PtCl<sub>6</sub>]<sup>2-</sup> or [PtCl<sub>4</sub>]<sup>2-</sup> ions in the solution and also the time of immersion. Columnar-shaped Pt clusters of relatively uniform size can be obtained, with coverage from submonolayer to multilayer. **Figure 5.1** is a representative ECSTM image of a Pt deposit obtained by immersing a freshly prepared Ru single crystal in an [PtCl<sub>6</sub>]<sup>2-</sup> solution. Clusters of 2-6 nm were obtained, with a slight preferential deposition of Pt on the Ru edges. The average height on Ru(0001) terraces is about 2 ML, while that on the edges is about 3 ML, yielding the total coverage of about 92%. Electroless deposition occurs only on freshly prepared Ru surfaces, a feature ascribed to the strongly bound OH groups that prevent or reduce electroless deposition when the Ru surface contacts an aqueous solution. The electroless process is tentatively ascribed to the local cell mechanism involving RuOH formation<sup>95</sup>. Interestingly, the driving force of the electroless deposition reaction is the difference in the equilibrium potentials of [PtCl<sub>6</sub>]<sup>2-</sup>, or [PtCl<sub>4</sub>]<sup>2-</sup> reduction and Ru oxidation. It is interesting that in the electroless deposition of Pd on Ru(0001) an atomic resolution of Pd(111) was obtained<sup>96</sup>.

Wieckowski et al. reported the spontaneous deposition Ru adlayers from RuO<sub>2</sub><sup>+</sup> solutions on three low-index Pt surfaces. The maximum coverage of Ru on these adlayer is about 20%<sup>97</sup>, and potential must be applied to reduce the Ru adlayer to metallic Ru. The Ru-decorated Pt nanoparticles showed considerable catalytic activity in the methanol-oxidation reaction<sup>57,98</sup>. We will discuss the catalytic properties of the Ru-decorated Pt nanoparticles in **section 5.3**.

### 5.1.1. Adsorption properties of Pt submonolayers on Ru(0001)

IR spectroscopy was used to obtain insights on the carbon monoxide absorption and oxidation mechanism on Pt-Ru electrocatalysts. **Figure 5.2** shows the SNIFTIR spectra of CO on submonolayer Pt deposits on Ru(0001). Two bipolar bands are clearly visible at potentials from 0.1 to 0.8 V. Analyses of IR spectra (*vide supra*) attributed the bipolar band at lower frequencies to blue-shifted CO (i.e., moved to higher frequency) on polycrystalline Ru<sup>5,81</sup>, whereas the higher-frequency bipolar band represents red-shifted CO on Pt(111).

Blyholder gave the first particle model of charge migration in the binding of CO<sup>99</sup>. The charge flows from the highest occupied CO orbital, 5σ, to empty *d*-orbitals on the metal atom. A negative formal charge on the metal atom is avoided by a postulated back-donation from the metal *d*<sub>π</sub> orbitals into the lowest unoccupied CO orbitals, 2π\*.

Theoretical methods (see below) later showed this simple model to be essentially valid, and it has proved useful in interpreting the adsorption of CO on Pt.

The modulation in the vibrational frequency of CO on Pt-Ru is attributed to the charge transfer from Ru to Pt, due to difference in work function that weakens the Ru-CO bond and strengthens the Pt-CO bond. The weaker bonding of Ru-CO on Pt-Ru makes CO more reactive here than on pure Ru, and accordingly, electro-oxidation sets in earlier in the potential scale. On the other hand, no significant charge transfer was found in a theoretical study of the electronic mechanism underlying the adsorption of CO on pure Pt, Ru, and on mixed Pt–M metal surfaces (M=Ru, Sn, Ge) with the relativistic density-functional self-consistent field method on clusters of ten atoms<sup>100</sup>. The presence of the metal weakened the Pt-C bond, therefore increasing CO tolerance, and also slightly lowered the CO stretching frequency of adsorbed carbon monoxide on Pt, although it was acknowledged that weakening the Pt-C bond would increase vibrational frequency by donation back-bonding. The promoting mechanism for bifunctional catalysis in alloying Pt with Ru, Sn, or Ge was attributed to lowering the dissociation energy of water, as well as modifying Pt-CO binding energy.

Density functional theory (DFT) demonstrated that the lowest CO bonding occurs in a Pt monolayer on an Ru(0001) surface<sup>101</sup>. Hammer and Nørskov's model revealed a weaker Pt-CO bond,<sup>102</sup> which includes a large transfer of *d* electrons from Pt to Ru, with the consequent shift of *d*-bands that lessens CO adsorption due to decreased back donation from Pt to antibonding CO orbitals. A parallelism was found in the change of adsorption energy with *d*-band center shifts for CO and H<sub>2</sub>, was suggesting some weakening of the H<sub>2</sub> chemisorption bond for a Pt monolayer on Ru surface that could reduce the kinetics of HOR<sup>103</sup>. The temperature-programmed desorption data for CO on Pt on Ru(0001) also indicate a decrease in the bonding strength of CO to Pt<sup>104</sup>. Furthermore, reactivity scales well with shifts in the center of *d*-band for strained crystals and overlayers, which could be operative for Pt islands given the ~4% lattice mismatch between Pt and Ru.

## 5.2. Pt deposition on Ru nanoparticles

The concept of a Pt monolayer catalyst was first verified with a Pt submonolayer on Ru substrate. This approach radically changed the design of the Pt-Ru catalysts and it is likely to similarly affect a broad range of catalysts. It facilitates an ultimate reduction of Pt loadings in Pt-Ru catalysts by depositing Pt only at the surface of Ru nanoparticles, so that the most of the Pt atoms become available for the catalytic reaction. Ru (10%) nanoparticles on Vulcan XC-72 carbon were heated in an H<sub>2</sub> atmosphere at ~300 °C for 2 h. This temperature is much lower than that required for bulk Ru preparation. After cooling down to room temperature, they were immersed in a solution of [PtCl<sub>4</sub>]<sup>2-</sup> ions for 30-60 minutes to obtain a bulk Pt:Ru ratio ranging from 1:20 to 1:5. The entire procedure was carried out in atmosphere of Ar or H<sub>2</sub>, and the amount of Pt available for electroless

deposition was controlled by the concentration and volume of the immersing solution. The area ratio of surface atoms to total atoms was calculated to be roughly 0.45 for 2.5 nm Ru particles<sup>105</sup>, so that the coverage ratio of Pt to Ru ranges from 1:9 to 1:2.

### 5.2.1. EXAFS and TEM characterization

Structural and electronic information can be inferred from *in situ* extended X-ray absorption fine structure (EXAFS) measurements<sup>106</sup>. **Figure 5.3a** presents Fourier transform of the Pt L<sub>3</sub> edge of the PtRu<sub>20</sub> catalyst at 0.1 V compared with that of carbon-supported Pt nanoparticles at 0.48 V in 1 M HClO<sub>4</sub>. The potential of the Pt-Ru catalyst was chosen so that the interaction of Pt with the adsorbed H<sub>2</sub>O and anions is the smallest, and hence, the perturbation of its electronic properties was expected to come predominantly from interaction with Ru atoms. The general appearance of the spectra is very different, with the Pt-Ru catalyst exhibiting the first large peak shifted to lower *r*-values due to Pt-Ru bonding. Fit of the data indicates that Pt is deposited in two-dimensional (2D) islands with Pt atoms coordinated with 3-4 Ru atoms, and the Pt-Ru length (0.269 nm) is the same as in Pt-Ru alloys. The latter finding further implies that Pt is bonded to Ru rather to RuOH.

The two-dimensional deposition of Pt was confirmed by comparing the Pt L<sub>3</sub> edge X-ray absorption near edge spectroscopy (XANES) spectra of the catalyst, held in the double layer region (at 0.40 V) with those of a reference Pt foil, **Fig. 5.3b**<sup>107</sup>. The absorption peaks (white lines) of the Pt submonolayer on Ru nanoparticles at the L<sub>3</sub> and L<sub>2</sub> edges are larger than the corresponding peaks for the Pt foil, indicating an increased *d*-band vacancy caused by the interaction between the Pt atoms and the Ru nanoparticle surface. Pt *5d*-band vacancies of 0.345 and 0.3 for PtRu<sub>20</sub> and Pt foil, respectively, were calculated<sup>108</sup>. The large increase in *d*-band vacancy confirms 2D growth because a smaller increase would be expected for three-dimensional (3D) clusters due to the effect of the atoms inside the clusters that are not in contact with Ru.

A prevailing view of carbon-supported metal nanoparticles is that they are in a form of cubo-octahedral or icosohedral structures<sup>105,109</sup>. One such model for the active electrocatalyst with submonolayer Pt coverage, a cubo-octahedral Ru particle with Pt islands on its surface, is shown as an inset in **Fig. 5.3b**. Pt atoms are in 2D islands as expected from EXAFS measurements and the Ru nanoparticles are supported on a high surface area Vulcan XC-72 carbon.

Transmission electron microscope (TEM) measurements determined the size of the metal particles after Pt electroless deposition. Because of the small amount of Pt relative to Ru, no attempt was made to locate the Pt atoms by using TEM chemical- and diffraction-analyses. Measurements of over a hundred metal particles from TEM images yielded an average diameter about 2.5 nm, only slightly larger than the 2 nm value as listed in E-TEK's specification for the Ru/C samples. Clearly, there is no significant agglomeration due to heating and Pt deposition. In the high-resolution images, ordered

atomic structures are seen. To identify the crystal structure of the particles, diffraction analysis was carried out on about 170 particles using a special computer routine based on fast Fourier transform of the lattice images of the particles. The symmetry and lattice spacing of the dominant features are consistent with the hexagonally close-packed Ru single crystal structure (**Fig. 5.4**).

### 5.2.2. H<sub>2</sub>/CO oxidation

In addition to having a good CO tolerance, Pt-Ru electrocatalysts must also have a high activity for H<sub>2</sub> oxidation. Comparison of the mass-specific activity of a PtRu<sub>20</sub> electrocatalyst with a commercial Pt-Ru 1:1 alloy electrocatalyst for the oxidation of pure H<sub>2</sub> showed that its activity is three times that of the commercial alloy. This indicates that even for a low Pt coverage on Ru, its activity for H<sub>2</sub> oxidation is preserved, a prerequisite for an active CO tolerant catalyst. Comparing the CO tolerance of the PtRu<sub>20</sub> electrocatalyst with that of two commercial Pt-Ru alloy electrocatalysts for the oxidation of 1095 ppm CO in H<sub>2</sub> confirmed the exceptional stability of the former (**Fig.5.5**); the measurements were obtained using a thin film rotating disk electrode at 2500 rpm at 60°C in 0.5 M H<sub>2</sub>SO<sub>4</sub>. The current drops to half the initial value after about 4 hours for PtRu<sub>20</sub>, while for the two commercial catalysts it happens in less than an hour. This enhanced CO tolerance of PtRu<sub>20</sub> is apparently due to a weakened CO adsorption on Pt/Ru and an efficient spill-over of CO from Pt sites to the surrounding Ru sites.

### 5.2.3. Fuel cell tests

Fuel-cell tests offer the ultimate verification of the usefulness of an electrocatalyst by determining its long-term stability under real operating conditions. They were performed on single cells using electrodes of 50 cm<sup>2</sup> and an anode catalyst loading of 0.2 mg cm<sup>-2</sup> total metal, corresponding to 0.18 mg Ru cm<sup>-2</sup> and 0.018 mg Pt cm<sup>-2</sup>; hence, the amount of Pt is approximately 1/10 of what is considered a standard anode loading for these tests. The cathode was a standard O<sub>2</sub> cathode with the Pt/C electrocatalyst. The fuel was clean H<sub>2</sub> or H<sub>2</sub> with 50 ppm of CO and 3% air (adding air is a routine procedure that helps CO oxidation at the electrode's surface). Excellent performance stability was seen. After 900 h of the constant current (0.4 A cm<sup>-2</sup>) test, no losses were observed with the cell operating on clean H<sub>2</sub>, or H<sub>2</sub> + 50 ppm CO + 3% air mixture. The cell was run with the latter fuel for a third of the total time. Switching between H<sub>2</sub> and H<sub>2</sub>/CO fuels entails small sharp changes in the cell's voltage, which produced spikes in the plot (**Fig. 5.6**). The effect of air bleed on CO tolerance was such that the catalyst worked well, even at contamination level of 100 ppm.

XANES data show that Pt in the PtRu<sub>20</sub> has 0.345 5d vacancy/atom. The back-bonding from the Pt to CO may decrease in this case, the likely reason for this catalyst's good CO tolerance. The weaker CO bonding on PtRu<sub>20</sub> than on Pt or the Pt-Ru alloy was

confirmed by CO stripping voltammetry. These data show that the electronic effect in Pt-Ru electrocatalysts may be more important than previously assumed.

These results clearly demonstrate that Pt submonolayers on Ru nanoparticles are stable during the fuel cell's operation and that this system represents a real catalyst. In addition to the high activity for H<sub>2</sub> oxidation and weak CO bonding, the strong segregation of Pt and Ru is a key factor that determines this catalyst's stability. Pt-Ru alloys represent a very strongly segregated system<sup>110</sup> in which Pt segregates to the surface, and is the origin of their inherent instability because the segregation essentially generates a Pt catalyst, which is poisoned by CO. Conversely, in the PtRu<sub>20</sub> catalyst, Pt islands are on the surface and no further segregation takes with usage; this explains the full retention of activity over 900 h. The data provide a powerful illustration of the possibility of nanoparticle surface modification by Pt monolayers as a method of obtaining low noble-metal loading of catalysts.

### 5.3 Methanol oxidation

As we pointed out for the Pt-Ru electrocatalysts, reviewing the work on methanol oxidation is beyond the scope of this article. We will briefly discuss some selected results with the electrocatalysts comprising a Pt submonolayer on Pt nanoparticles<sup>111</sup> and Ru-decorated Pt nanoparticles. The direct methanol fuel cell is a potential candidate as a noteworthy power source for mobile devices because of its high energy density per unit volume and immediate reuse by refueling. Methanol has a high energy density, with full oxidation to CO<sub>2</sub> occurring through a six-electron reaction, and is a promising choice for energy applications, for instance, in portable electronics. Its attractive properties include availability, ease of handling and storage. The obstacles against the implementing DMFCs are the insufficient activity of the catalysts employed so far, and high cost of Pt in platinum-based bimetallic catalysts.

Bewick et al.<sup>112</sup> identified CO as the species that acts as a catalytic poison and inhibits further oxidation of methanol on Pt electrodes. The reactive intermediate is a formate species, HCOO that generates asymmetric COO vibration around 1300 cm<sup>-1</sup>, leading to an increase in the methanol oxidation current after CO oxidation<sup>113</sup>. Recently, water molecules were detected adsorbed on the Ru sites on Ru and Pt-Ru (but not on Pt) catalysts, and were assigned as the oxygen donor to the methanol adsorbates that promote methanol oxidation<sup>114</sup>. This was considered as directly supporting the “bi-functional mechanism” of Pt-Ru catalysts for the methanol-oxidation reaction.

Methanol oxidation proceeds with the progressive dehydrogenation of the organic molecule on the anode surface, viz:



Pt has the highest adsorption of methanol on its surface, but its catalytic properties are low due to the formation of ‘poison’ species (most notably CO) that can be oxidized only after the Pt is covered with OH. Platinum-based bimetallic electrocatalysts, such as Pt-Ru alloys and Ru-decorated Pt materials, are the most active ones. The bi-functional mechanism is to a large extent operative in these catalysts. Most commercial Pt-Ru catalysts are based on 1:1 Pt-Ru alloy. While the alloys typically show enhanced activity in comparison with pure Pt, there is significant Pt loading in the bulk of the alloy in which catalysis does not proceed because the sites are inaccessible for methanol adsorption; hence, the need for reducing the Pt content.

**Figure 5.7** shows the oxidation of methanol on a submonolayer of Pt on Ru, Pt<sub>3.9</sub>Ru<sub>10</sub>/C (3.9 μg cm<sup>-2</sup> Pt), and commercial PtRu/C (10 μg cm<sup>-2</sup> Pt) electrocatalysts. The Pt-mass specific activity (current) of the monolayer-level electrocatalyst is several times higher than that of a commercial sample.

Wieckowski et al.<sup>97,98</sup> investigated in detail properties of the Ru-decorated Pt surfaces obtained by spontaneous deposition. These studies were reviewed recently<sup>115</sup>; here we give a brief summary. Several methods were used to obtain Ru-modified Pt surfaces, including electrodeposition of Ru ad-atoms, electrochemical<sup>116,117</sup>, spontaneous deposition<sup>118,57</sup>, UHV deposition<sup>119</sup> and organometallic chemistry<sup>120</sup>. However, these various methodologies produce different amounts of metallic vs. oxidized Ru atoms, engendering different electrochemical activity of the Pt-Ru system. The amount of Ru deposited was monitored by AES, XPS or *in-situ* STM, or by following the difference of the voltammetric peak currents in the double-layer range. The increase of electrochemical activity of Ru-decorated Pt surfaces relies on the bifunctional mechanism and the decrease of CO-binding energy on Pt atoms that are in close proximity to the Ru islands. In contrast to FTIR measurements on optimized Pt-Ru alloys where only one linearly bonded CO peak is visible, the Ru submonolayers on Pt(hkl) show two linearly bonded CO peaks (one for CO-Pt and one for CO-Ru)<sup>121</sup>. It was later confirmed that Ru is deposited in form of islands with a minimal size of about eight atoms; this minimal cluster size was shown to be needed for the appearance of the Ru-CO IR peak<sup>122</sup>. The existence of the two peaks is attributed to slow CO oxidation kinetics, but it is unclear whether the reaction limiting step reflects the slow diffusion of CO towards the reactive Pt-Ru sites, or the slow change in the oxidation state of Ru that, in turn, reduces the speed of delivery of the OH species required for the reaction.

The growth of Ru islands on Pt(hkl) was found to be substrate-dependent, so that the Ru layer is almost completely in the form of a monolayer on Pt(110), whereas the two- and three- dimensional growth is facilitated on the other two low-index Pt surfaces, especially on Pt(111)<sup>123</sup>. The Ru-Pt(111) is more effective catalyst for methanol oxidation<sup>124</sup> than the other two surfaces decorated with Ru, because the edge of a Ru island is the active site in methanol oxidation; therefore, controlling the extent of the multidimensional islands is of a particular importance for fuel cell catalysis<sup>125</sup>.

## 6. Conclusions

Knowledge of the electrochemistry and electrocatalysis of Ru has significantly progressed since the turn of the millenium when a quick method for preparing well-ordered single crystal Ru electrodes was introduced. Considerable structural effects were observed for several reactions on single crystal and polycrystalline Ru surfaces. The densest packing of Ru atoms, i.e., the (0001) surface that is protected from oxidation by chemisorbed bisulfate species at low potentials, stays impervious to oxygen penetration, and has low catalytic activity towards CO oxidation, hydrogen oxidation, and oxygen reduction. In sharp contrast, the more open structure of (10 $\bar{1}$ 0) shows no measurable coverage of sulfate/bisulfate species, the shape of the voltammetry profiles dramatically change upon cycling, and its catalytic activities are several times higher than on the Ru(0001) surface.

Initial stages of Ru oxidation, involving RuOH formation by the oxidation of H<sub>2</sub>O and the distinction of that reaction from H adsorption seems now well understood. Random formation of RuO<sub>2</sub> islands on the smooth OH-covered Ru(0001) surface under electrochemical conditions was observed without place exchange by *in situ* STM and X-ray scattering measurements.

Fuel cell electrocatalysis also has advanced significantly with innovations in the preparation of active Pt-Ru catalysts. A new type of electrocatalyst was developed, consisting of a Pt submonolayer on Ru nanoparticles. It has high CO tolerance and a very low Pt content. Its synthesis was facilitated by the discovery of electroless deposition of Pt on Ru nanoparticles that can be controlled so that most (> 90%) Pt atoms become available for the catalytic reaction. The catalytic activity of PtRu<sub>20</sub> prepared by this method affords considerable advantages in the oxidation of H<sub>2</sub>, CO, and CH<sub>3</sub>OH compared with commercial Pt-Ru alloys.

While the experimental data has mounted, theoretical elucidations of the observed phenomena also made significant progress. There are, however, still open basic questions. The difference in behavior of single-crystal surfaces is not well understood. Similarly, there is a need to alter the simple bifunctional mechanism to reflect changes in the adsorption bond of metal-CO, as well as in the electronic structure of the Pt-Ru catalyst.

The rich chemical properties of Ru are replicated in its fascinating surface electrochemical and catalytic properties. For this reason, Ru and its alloys are likely to remain in focus of the research in catalysis and electrocatalysis for the foreseeable future.

## Figure Captions:

**Fig. 1.1.** Structural model of (a) Ru(0001); (b) two terminations of the Ru(10 $\bar{1}$ 0) surface.

**Fig. 3.1.** Voltammetry curves for (a) polycrystalline Ru and Ru(0001) in 1 M H<sub>2</sub>SO<sub>4</sub>, and, (b) oxidation with different positive potential limits in 0.05 M H<sub>2</sub>SO<sub>4</sub>. Sweep rates: (a) 10 mV s<sup>-1</sup>, and (b) 20 mV s<sup>-1</sup>.

**Fig. 3.2.** Voltammetry curves for the Ru(0001) surface oxidation in (a) 0.1 M HClO<sub>4</sub> and (b) 0.1 M NaOH. Sweep rates: (a) 50 mV s<sup>-1</sup> and (b) 20 mV s<sup>-1</sup>. The inset in (a) shows the charge associated with the displacement of adsorbed species at 0.12 V by the adsorption of CO.

**Fig. 3.3.** Voltammetry curves for the Ru(10 $\bar{1}$ 0) surface in (a) 0.05 M H<sub>2</sub>SO<sub>4</sub> and (b) 0.1 M HClO<sub>4</sub>. Sweep rates: (a) 20 mV s<sup>-1</sup> and (b) 50 mV s<sup>-1</sup>. The insert in (b) shows the charge associated with the peaks in the positive scan, obtained by peak fitting routine.

**Fig. 3.4** Proposed structural models for Ru(0001) oxidation, where the O, S, and Ru atoms are represented by the open, lightly-shaded, and heavily- shaded circles, respectively. The layer spacings are given in nm, and coverage is given in monolayers.

**Fig. 3.5.** *In-situ* infrared spectra obtained from (a) polycrystalline Ru, and (b) Ru(0001) electrode in 0.05 M H<sub>2</sub>SO<sub>4</sub>. The reference spectrum is obtained at 0.03 V, and sample spectra are taken every 0.1 V, from 0.05 to 0.85 V. 4096 scans were co-added in 16 cycles, 256 scans each; the resolution was 8 cm<sup>-1</sup>. Spectra are offset for clarity.

**Fig. 3.6.** ECSTM images of the chemically oxidized Ru(0001) obtained in 0.05 M H<sub>2</sub>SO<sub>4</sub> at open circuit conditions (~0.95 V). (a) 700 x 700 nm, Z range 3 nm; and, (b) 5.8 x 5.8 nm.

**Fig. 3.7.** a) Schematic view of the surface structure of an ideal RuO<sub>2</sub>(110) single-crystal, where solid circles represent Ru atoms in the surface plane, open circles O atoms in the surface plane, and dotted open circles O atoms below surface plane; b) model of an ideal RuO<sub>2</sub>(110) single-crystal. The RuO<sub>2</sub>(110) surface contains two kinds of coordinatively unsaturated (CUS) atoms: two-fold bridging O (O<sub>br</sub>) and five-fold Ru (Ru<sub>CUS</sub>). The O<sub>3F</sub> is the O atoms that lay in the plane in the Ru atoms and posses its bulk-like three-fold coordination.

**Fig. 3.8.** ECSTM images of the oxidation of Ru(0001) in 0.05 M H<sub>2</sub>SO<sub>4</sub> at (a) 1.0 V, (b) 1.17 V, (c) 1.27 V, and (d) 1.35 V. Image (a) 500 x 500 nm, Z range 2 nm, inset of (a) 4 x 4 nm; (b) 230 x 230 nm, Z range 2 nm, inset of (b) 20 x 20 nm, Z range 2 nm; (c) 165 x 165 nm, Z range 10 nm; and, (d) 250 x 250 nm, Z range 10 nm.

**Fig. 4.1.** Hydrogen oxidation on rotating Ru(0001) and Ru(10 $\bar{1}$ 0) electrodes in an H<sub>2</sub>-saturated 0.05 M H<sub>2</sub>SO<sub>4</sub> solution at three different temperatures. Sweep rate 20 mV s<sup>-1</sup>; rotation rate 900 rpm.

**Fig. 4.2.** STM image of the Ru(0001) surface after slight mechanical polishing with 0.05  $\mu$ m alumina slurry, starting from a well-ordered single-crystal surface. Image size 100 x 100 nm, Z range 8 nm.

**Fig. 4.3.** Voltammetric curves for CO oxidation on the Ru(10 $\bar{1}$ 0) and Ru(0001) surfaces in CO-saturated 0.1 M H<sub>2</sub>SO<sub>4</sub> solution. Sweep rate 20 mV s<sup>-1</sup>.

**Fig. 4.4.** *In situ* FTIR spectra collected from the Ru(0001) electrode in 0.1 M HClO<sub>4</sub> solution at 20 °C during a potential step experiment after the adsorption of CO. The CO was pre-adsorbed at -200 mV, after which the solution was sparged with N<sub>2</sub>, the potential was then stepped up to +1100 mV in 25 mV increments, with further spectra collected at each step. The spectra showing the CO<sub>2</sub> absorption were normalized to the first spectrum, collected at -200 mV. The spectra showing the CO absorption were normalized to a spectrum taken after holding the potential at +1100 mV for 2 min at the end of the experiment, to ensure the electrode surface was free of adsorbed CO. Some of the spectra collected are omitted for the sake of clarity. Figure is taken from reference. Potentials are referenced against Ag/AgCl,Cl<sup>-</sup> electrode.

**Fig. 4.5.** *In situ* IR spectra of CO oxidation at the Ru(10 $\bar{1}$ 0) surface at different potentials in CO-saturated 0.1 M H<sub>2</sub>SO<sub>4</sub> solution. 128 scans with 4 cm<sup>-1</sup> resolution are collected in a single step. Background scan was obtained at 1.1 V.

**Fig. 4.6.** Rotating disk-ring electrode measurements for O<sub>2</sub> reduction on Ru(10 $\bar{1}$ 0) in 0.1 M HClO<sub>4</sub>. Sweep rate 20 mV s<sup>-1</sup>; ring potential E=1.2 V; disc area 0.282 cm<sup>2</sup>; rotation rates are indicated in the graph. The insert shows the log j / (j<sub>d</sub> - j) vs. E plot obtained for 1600 rpm.

**Fig. 5.1.** STM image of an electroless (spontaneous) Pt adlayer deposited on Ru(0001) in 0.01 M H<sub>2</sub>PtCl<sub>6</sub> + 0.1 M H<sub>2</sub>SO<sub>4</sub> solution. Image recorded at open circuit potential in 0.1 M H<sub>2</sub>SO<sub>4</sub>. Image size 100 x 100 nm, Z range 2 nm.

**Fig. 5.2.** SNIFTIRS spectra for a Ru(0001) electrode with a submonolayer of Pt in a CO-saturated 0.1 M H<sub>2</sub>SO<sub>4</sub> solution. The reference spectrum is obtained at 0.075 V and the sample spectra are taken from 0.10 V incremented by 0.1 V up to 0.80 V. 8192 scans were co-added in 16 cycles, 512 scans each; the resolution was 8 cm<sup>-1</sup>. Spectra are offset

for clarity.

**Fig. 5.3.** (a) EXAFS FT ( $k^3$ -weighted) of Pt  $L_3$ -edge of the catalyst sample compared with *fcc* Pt. (b) *In situ* XANES spectra at the Pt  $L_3$  of the PtRu<sub>20</sub> electrocatalyst held at 0.40 V in 1 M HClO<sub>4</sub> electrolyte solution. The spectra were obtained in a fluorescence mode. The spectra of the Pt foil used as a reference and in the calculation of the *d*-band vacancies; Insert in (b) shows a cubo-octahedral particle model for the electrocatalyst consisting of the Ru particle with two-dimensional Pt islands on its surface.

**Fig 5.4.** Electron micrographs of the PtRu<sub>20</sub> catalyst made by spontaneous deposition of Pt on Ru nanoparticles. (a) Low magnification morphology of the metal particles (black dots, average size 2.5 nm) on carbon spheres (average size 50 nm). (b - d) High-resolution images showing atomic resolved lattice structures. (e) Diffractogram obtained from the high-resolution image shown in (d) with measured the angles and lattice spacings that are consistent with *hcp* Ru single crystal structure.

**Fig. 5.5.** Comparison of the CO tolerance of three catalysts based on the current as a function of time for the oxidation of H<sub>2</sub> with 1095 ppm of CO at 60 °C for the PtRu<sub>20</sub>, and two commercial electrocatalysts at 0.05 V with the loadings indicated in the graph. A considerably larger CO tolerance is seen for the PtRu<sub>20</sub> (1% Pt, 10% Ru on C) electrocatalyst.

**Fig. 5.6.** Long-term test of the performance stability of the PtRu<sub>20</sub> electrocatalyst in an operating fuel cell. The fuel cell voltage at constant current of 0.4 A cm<sup>-2</sup> is given as a function of time for the electrode of 50 cm<sup>2</sup> with an anode containing to 0.18 mg Ru cm<sup>-2</sup> and 0.018 mg Pt cm<sup>-2</sup>; (approximately 1/10 of the standard Pt loading) and a standard air cathode with a Pt/C electrocatalyst. The fuel was clean H<sub>2</sub> or H<sub>2</sub> with 50 ppm of CO and 3% air; temperature 80 °C.

**Fig. 5.7.** Oxidation of methanol on a submonolayer of Pt on Ru i.e. Pt<sub>3.9</sub>Ru<sub>10</sub>/C (3.9 μg cm<sup>-2</sup> Pt), and commercial PtRu/C (10 μg cm<sup>-2</sup> Pt) electrocatalysts in 0.5 M CH<sub>3</sub>OH + 0.1 M H<sub>2</sub>SO<sub>4</sub>; sweep rate of 50 mV s<sup>-1</sup>; room temperature. The currents presented are normalized by Pt mass.

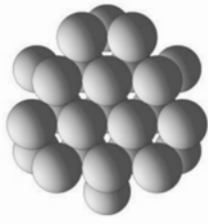
## References

- <sup>1</sup> S. Trasatti, W.E. O'Grady in: *Advances in Electrochemistry and Electrochemical Engineering*, Vol. 12, Ed. by H. Gersher, C. Tobias, Wiley, New York, 1982.
- <sup>2</sup> S. Gottesfeld, T. Zawodzinski in: *Advances in Electrochemical Science and Engineering*, Vol. 5, Ed. by D.M. Kolb, R. Alkire, VCH, New York, 1982.
- <sup>3</sup> P. N. Ross in: *Electrocatalysis*, Ed. by J. Lipkowski, P. N. Ross, Wiley-VCH, New York, 1998.
- <sup>4</sup> T.E. Madley, H.A. Engelhardt and D. Manzel, *Surf.Sci.* **48** (1975) 304.
- <sup>5</sup> N.S. Marinkovic, J.X. Wang, H. Zajonz and R.R. Adzic, *Electrochemical and Solid State Letters* **3** (2000) 508.
- <sup>6</sup> N. Ikemiya T. Senna and M. Ito, *Surf.Sci.* **464** (2000) L681.
- <sup>7</sup> H. Inoue, J.X. Wang, K. Sasaki and R.R. Adzic, *J.Electroanal.Chem.* **554** (2003) 77.
- <sup>8</sup> H. Inoue, S.R. Brankovic, J.X. Wang and R.R. Adzic, *Electrochim.Acta* **47** (2002) 3777.
- <sup>9</sup> P.C.Liu, C.H.Yang, S.L.Yau and M.S.Zei, *Langmuir* **18** (2002) 754.
- <sup>10</sup> M.B.Vukmirovic, R.L.Sabatini and R.R.Adzic, *Surf.Sci* **572** (2004) 269.
- <sup>11</sup> S. Hadzi-Jordanov, H. Angerstein-Kozłowska, M. Vukovic and B.E. Conway, *J. Electrochem. Soc.* **125** (1978) 1569.
- <sup>12</sup> D. Michell, D.A.J. Rand and R. Woods, *J. Electroanal. Chem.* **89** (1978) 11.
- <sup>13</sup> N.A. Anastasijevic, Z.M. Dimitrijevic and R.R. Adzic, *J. Electroanal. Chem.* **199** (1986) 351.
- <sup>14</sup> V. Horvat-Radosević, K. Kvastek, M. Vuković, B. Čukman, *J.Electroanal.Chem.* **482** (2000) 188.
- <sup>15</sup> R.C. Walker, M. Bailes and L.M. Peter, *Electrochim.Acta* **44** (1998) 1289.
- <sup>16</sup> N.S. Marinkovic, J.X. Wang, H. Zajonz and R.R. Adzic, *J.Electroanal.Chem.* **500** (2001) 388.
- <sup>17</sup> J.X. Wang, N.S. Marinkovic, H. Zajonz, B.M. Ocko and R.R. Adzic, *J.Phys.Chem. B* **105** (2001) 2809.
- <sup>18</sup> S.R. Brankovic, J.X. Wang, Y. Zhu, R. Sabatini, J. McBreen and R.R. Adzic, *J.Electroanal.Chem.* **524-525** (2002) 231.
- <sup>19</sup> W.F. Lin, P.A. Christensen, A. Hamnett, M.S. Zei and G. Ertl, *J.Phys.Chem. B* **104** (2000) 6642.
- <sup>20</sup> W. F.Lin, P.A. Christensen and A. Hamnett, *Phys.Chem.Chem.Phys.* **3** (2001) 3312.
- <sup>21</sup> W.F. Lin, P.A. Christensen and A. Hamnett, *J.Phys.Chem. B* **104** (2000) 12002.
- <sup>22</sup> E.Y. Cao, D.A. Stern, J.Y. Gui and A.T. Hubbard, *J.Electroanal.Chem.* **354** (1993) 71.
- <sup>23</sup> W.F. Lin, M.S. Zei, Y.D. Kim, H. Over and G. Ertl, *J.Phys.Chem. B* **104** (2000) 6040.
- <sup>24</sup> M.S. Zei and G. Ertl, *Phys.Chem.Chem.Phys.* **2** (2000) 3855.
- <sup>25</sup> W.B. Wang, M.S. Zei and G. Ertl, *Phys.Chem.Chem.Phys.* **3** (2001) 3307.
- <sup>26</sup> W.B. Wang, M.S. Zei and G. Ertl, *Chem.Phys.Lett.* **355** (2002) 301.
- <sup>27</sup> J. Lee, W.B. Wang, M.S. Zei and G. Ertl, *Phys.Chem.Chem.Phys.* **4** (2002) 1393.
- <sup>28</sup> A.M. El-Aziz and L.A. Kibler, *Electrochem.Comm.* **4** (2002) 866.
- <sup>29</sup> H. Hoster, B. Richter and R.J. Behm, *J.Phys.Chem B* **108** (2004) 14780.
- <sup>30</sup> R.R. Adzic, F. Feddrix and E. Yeager, *J.Electroanal.Chem.* **341** (1992) 287.
- <sup>31</sup> N.A. Anastasijevic, Z.M. Dimitrijevic and R.R. Adzic, *Electrochim.Acta* **31** (1986) 1125.
- <sup>32</sup> J. Prakash and H. Joachin, *Electrochim.Acta* **45** (2000) 2289.
- <sup>33</sup> H.D. Abruna (Ed), *Electrochemical Interfaces*, VCH New York 1991.
- <sup>34</sup> F.C. Nart, T. Iwasita and M. Weber, *Electrochim.Acta* **30** (1994) 961.
- <sup>35</sup> P.C. Lu, C.H. Yang S.L. Lau and M.S. Zei, *Langmuir* **18** (2002) 754 and references therein.
- <sup>36</sup> P.W. Faguy, N.S. Marinkovic and R.R. Adzic, *Langmuir* **12** (1996) 243.
- <sup>37</sup> K. Kunimatsu, M.G. Samant and H. Seki, *J.Electroanal.Chem.* **258** (1989) 163.
- <sup>38</sup> F.C. Nart and T. Iwasita, *J.Electroanal.Chem.* **322** (1992) 289.
- <sup>39</sup> P.W. Faguy, N.S. Marinkovic and R.R. Adzic, *J.Electroanal.Chem.* **407** (1996) 209.
- <sup>40</sup> W. Savich, S.G. Sun, J. Lipkowski and A. Wieckowski, *J.Electroanal.Chem.* **388** (1995) 233.
- <sup>41</sup> M. Nakamura, Y. Sakurai and M. Ito, *J.Electroanal.Chem.* **563** (2004) 63.
- <sup>42</sup> T. Senna, N. Ikemiya and M. Ito, *J.Electroanal.Chem.* **511** (2001) 115.
- <sup>43</sup> N.S. Marinkovic, J.S. Marinkovic and R.R. Adzic, *J.Electroanal.Chem.* **467** (1999) 291.
- <sup>44</sup> J. Lipkowski, Z. Shi, A. Chen and B. Pettinger, *ElectrochimActa* **43** (1998) 2875.
- <sup>45</sup> N.S. Marinkovic, J.X. Wang, J.S. Marinkovic and R.R. Adzic, *J.Phys.Chem. B* **103** (1999) 139.
- <sup>46</sup> Z. Shi, J. Lipkowski, M. Gamboa, P. Zelenay and A. Wieckowski, *J.Electroanal.Chem.* **366** (1994) 317.
- <sup>47</sup> V.B. Paulissen and C. Korzeniewski, *J.Electroanal.Chem.* **351** (1993) 329.
- <sup>48</sup> R.M. Hammaker, A. Francis, R.P. Eischens, *Spectrochim.Acta* **21** (1965) 1295.
- <sup>49</sup> K. Ashley, S. Pons, *Chem. Rev.* **88** (1988) 673.
- <sup>50</sup> S.D. Ross, *Inorganic Infrared and Raman Spectra*, McGraw-Hill, Maidenhead, UK 1972.
- <sup>51</sup> J.K. Foley, C. Korzeniewski, J.L. Daschbach and S. Pons in: *Electroanalytical Chemistry*, Vol 14, Ed. by A.J. Bard, Marcel Dekker, New York 1986.
- <sup>52</sup> Y. Shingaya and M. Ito, *J.Electroanal.Chem.* **467** (1999) 299.
- <sup>53</sup> Y. Sawatari, J. Inukai and M. Ito, *J.Electron Spectrosc. Related Phenomena* **64-65** (1993) 515.

- <sup>54</sup> T. Iwasita, F.C. Nart in: *Advances in Electrochemical Science and Engineering*, Vol 4, Ed. by H. Gerisher, C. Tobias, Verlag, Weinheim (1995).
- <sup>55</sup> H. Over, *Prog.Surf.Sci.* **58** (1998) 249.
- <sup>56</sup> H. Over, *Appl.Phys. A* **75** (2002), 37.
- <sup>57</sup> W. Chrzanowski and A. Wieckowski, *Langmuir* **13** (1997) 5974.
- <sup>58</sup> J.K. Norskov, T. Bligaard, A. Logadottir, S. Bahn, L.B. Hansen, M. Bollinger, H. Benggaard, B. Hammer, Z. Šljivančanin, M. Mavrikakis, Y. Xu, S. Dahl, C.J.H. Jacobsen, *J Catal.* **209** (2002) 275–278.
- <sup>59</sup> I. J. Malik and J. Hrbek, *J.Phys.Chem.* **95**, (1991) 10188.
- <sup>60</sup> A. Bottcher and H. Niehus, *J.Chem.Phys.* **110**, (1999) 3186.
- <sup>61</sup> C. Stampfl, S. Schwegmann, H. Over, M. Scheffler, and G. Ertl, *Phys.Rev.Lett.* **77** (1996) 3371.
- <sup>62</sup> A. Bottcher, H. Niehus, S. Schwegmann, H. Over and G. Ertl, *J.Phys.Chem. B* **101** (1997) 11185.
- <sup>63</sup> A. Bottcher, M. Rogazia, H. Niehus, H. Over, G. Ertl, *J.Phys.Chem.* **103** (1999) 6267.
- <sup>64</sup> H. Over, Y. D. Kim, A. P. Seitsonen, S. Wendt, E. Lundgren, M. Schmid, P. Varga, A. Morgante and G. Ertl, *Science* **287** (2000) 1474.
- <sup>65</sup> H. Madhavaram, H. Idriss, S. Wendt, Y. D. Kim, M. Knapp, H. Over, J. Aßmann, E. Löffler, and M. Muhler, *J.Catal.* **202** (2001) 296.
- <sup>66</sup> Lj. Atanasoska, W.E. O’Grady, R.T. Atanasoski, F.H. Pollak, *Surf.Sci.* **202** (1988) 142.
- <sup>67</sup> H. Over, A.P.Seitsonen, E. Lundgren, M. Schmid and P. Varga, *Surf.Sci.* **515** (2002) 143.
- <sup>68</sup> M. Pourbaix (Ed.), *Atlas of Electrochemical Equilibria in Aqueous Solutions*, NACE, Houston, TX, 1974.
- <sup>69</sup> F. Ludwig, R.K. Sen and E.B. Yeager, *Elektrokhimiya* **13** (1977) 847.
- <sup>70</sup> B.E. Conway and L. Bai, *J.Electroanal.Chem.* **198** (1986) 149.
- <sup>71</sup> H. Gasteiger, N.M. Markovic and P.N. Ross, *J.Phys.Chem.* **99** (1995) 8290.
- <sup>72</sup> J. Wang, S.R. Brankovic, Y. Zhu, J.C. Hanson and R.R. Adzic, *J.Electrochem.Soc.* **150** (2003) A1108.
- <sup>73</sup> H.A. Gasteiger, N.M. Markovic, P.N. Ross and E.J. Cairns, *J.Phys.Chem.* **97** (1993) 12020.
- <sup>74</sup> H. Over and M. Muhler, *Prog.Surf.Sci.* **72** (2003) 3.
- <sup>75</sup> R.L.C. Wang, H.J. Kreuzer, P. Jakob and D.J. Menzel, *J.Chem.Phys.* **111** (1999) 2115.
- <sup>76</sup> P. He, H. Dietrich and K. Jacobi, *Surf.Sci.* **345** (1996) 241.
- <sup>77</sup> C. H. F. Peden and D. W. Goodman, *J.Phys.Chem.* **90**, (1986) 1360.
- <sup>78</sup> A. Botcher and H. Conrad, *J.Chem.Phys.* **112** (2000) 4779.
- <sup>79</sup> A. Bottcher and H. Niehus, *Phys. Rev. B* **60** (1999) 14396.
- <sup>80</sup> H.A. Gasteiger, P.N. Ross and E.Cairns, *J. Surf. Sci* **293**, (1993) 67.
- <sup>81</sup> W.F. Lin, M.S. Zei, M. Eiswirth, G. Ertl, T. Iwasita and W. Vielstich, *J.Phys.Chem. B* **103** (1999) 6968.
- <sup>82</sup> S.R. Brankovic, N.S. Marinkovic, J.X. Wang and R.R. Adzic, *J.Electroanal.Chem.* **532** (2002) 57.
- <sup>83</sup> M.B. Vukmirovic, unpublished results.
- <sup>84</sup> J.M.Jin, W.F.Lin and P.A.Christensen, *J.Electroanal.Chem.* **563** (2004) 71.
- <sup>85</sup> O.A.Petrii, *Doklady AN SSSR* **160** (1965) 871.
- <sup>86</sup> J.O’M. Bockris, H. Wroblowa, *J. Electroanal. Chem.*, **7**, (1964) 428 .
- <sup>87</sup> M. Watanabe, S. Motoo, *J.Electroanal.Chem.* **60** (1975) 267.
- <sup>88</sup> M.Watanabe, M. Uchida, S. Motoo, *J.Electroanal.Chem.* **229** (1987) 395.
- <sup>89</sup> A.N. Haner, P.N. Ross Jr., *J.Phys.Chem.* **95** (1991) 3740.
- <sup>90</sup> B.N. Grgur, N.M. Markovic, P.N. Ross, *J.Electrochem. Soc.* **146** (1999) 1613.
- <sup>91</sup> M. Krausa, W. Vielstich, *J.Electroanal.Chem.* **379** (1994) 307.
- <sup>92</sup> J. McBreen, S. Mukerjee, *J.Electrochem.Soc.* **142** (1995) 3399.
- <sup>93</sup> S. R. Brankovic, J. X. Wang and R. R. Adzic, *Electrochem. Solid State Lett.* **4** (2001) A217.
- <sup>94</sup> S.R. Brankovic, J. McBreen, R.R. Adzic, *J.Electroanal.Chem.* **503** (2001) 99.
- <sup>95</sup> J. Clavilier, J.M. Feliu, A. Aldaz, *J.Electroanal.Chem.* **243** (1988) 419.
- <sup>96</sup> S.R. Brankovic, J. McBreen, R.R. Adzic, *Surf.Sci.* **479** (2001) L363.
- <sup>97</sup> W. Chrzanowski, H. Kim, A. Wieckowski, *Catal.Lett.* **50** (1998) 9.
- <sup>98</sup> G Tremiliosi-Fuho, H. Kim, W. Chrzanowski, A. Wieckowski, B. Grzybowska, P. Kulesza, *J.Electroanal.Chem.* **467** (1999) 143.
- <sup>99</sup> G. Blyholder, *J.Phys.Chem.* **68** (1964) 2772.
- <sup>100</sup> M-S. Liao, C. R. Cabrera and Y. Ishikawa, *Surf. Sci.* **445** (2000) 267.
- <sup>101</sup> M.T.M.Kopper, T.E.Shubina and R.A.vanSanten, *J. Phys. Chem. B* **106** (2002) 686.
- <sup>102</sup> B.Hammer and J.K.Norskov, *Adv.Catal.* **45** (2000) 71.
- <sup>103</sup> E.Christoffersen, P.Liu, A.Ruban, H.L.Skiver and J.K.Norskov, *J.Catal.* **199** (2001) 123.
- <sup>104</sup> F. Buatier de Mongeot, M. Scherer, B. Gleich, E. Kopatzki, and R. J. Behm, *Surf. Sci.* **411**, (1998) 249.
- <sup>105</sup> R.E. Benfield, *J.Chem.Soc. Faraday Trans.* **88** (1992) 1107.
- <sup>106</sup> K.Sasaki, Y.Mo, J.X.Wang, M.Balasubramanian, F.Uribe, J.McBreen and R.R.Adzic, *Electrochim.Acta* **48** (2003) 3841.

- 
- <sup>107</sup> K. Sasaki, J.X. Wang, M. Balasubramanian, J. McBreen, F. Uribe and R.R. Adzic, *Electrochim.Acta* **49** (2004) 3873.
- <sup>108</sup> A.N. Mansour, J.W. Cook, D.E. Sayers, *J.Phys.Chem.* **88** (1984) 2330.
- <sup>109</sup> K. Kinoshita, in: *Modern Aspects of Electrochemistry*, Vol. 14, Ed. by J.O'M. Bockris, B.E. Conway, R.E. White, Plenum, New York, 1982.
- <sup>110</sup> A.V. Ruban, H.L. Skriver and J.K. Nørskov, *Phys.Rev B* **59** (1999) 15990.
- <sup>111</sup> K. Sasaki, M. Shao, M.B. Vukmirovic and R.R. Adzic, *ECS Meeting Abstracts*, Denver, CO, May 7-11, 2006, p. 1103.
- <sup>112</sup> B. Beden, C. Lamy, A. Bewick, K. Kunimatsu, *J.Electroanal.Chem.* **121** (1981) 343.
- <sup>113</sup> Y.X. Chen, A. Miki, S. Ye, H. Sakai, M. Osawa, *J.Am.Chem.Soc.* **125** (2003) 3680.
- <sup>114</sup> T. Yajima, H. Uchida, M. Watanabe, *J.Phys.Chem. B* **108** (2004) 2654.
- <sup>115</sup> F.Mallard, G.-Q. Lu, A.Wieckowski and U.Stimming, *J.Phys.Chem. B* **109** (2005) 16230.
- <sup>116</sup> E. Herrero, K. Fraszczuk and A. Wieckowski, *J.Electroanal.Chem.* **361** (1993) 269.
- <sup>117</sup> S. Cramm, K. Fiedrich, K.P. Geyzers, U. Stimming and R.Vogel, *J.Anal.Chem.* **358** (1997) 189.
- <sup>118</sup> M.M.P. Jansen and J. Moolhusen, *Electrochim.Acta* **21** (1976) 861.
- <sup>119</sup> H. Hoster, T. Iwasita, H. Baumgartner and W. Vielstich, *J.Electrochem.Soc.* **148** (2001) A496.
- <sup>120</sup> C.E Lee and S.H. Bergens, *J.Phys.Chem. B* **102** (1998) 193.
- <sup>121</sup> K.A. Friedrich, K.P. Geyzers, U. Linke, U. Stimming and J. Stumper, *J.Electroanal.Chem.* **402** (1996) 123.
- <sup>122</sup> S.Z. Zou, I. Villegas, C. Stuhlmann and M.J. Weaver, *Electrochim.Acta* **43** (1998) 2811.
- <sup>123</sup> A.Crown, C.Johnson and A.Wieckowski, *Surf.Sci.Lett.* **506** (2002) L268.
- <sup>124</sup> G.Tremiliosi-Filho, H.Kim, W.Xhrzanowski, A.Wietzkowski, B.Grzybowska and P.Kulezsa, *J.Electroanal.Chem.* **467** (1999) 143.
- <sup>125</sup> E. Herrero, J.M. Feliu and A. Wietzkowski, *Langmuir* **15** (1999) 4944.

**a) Ru(0001)**



**b) Ru(10 $\bar{1}$ 0)**

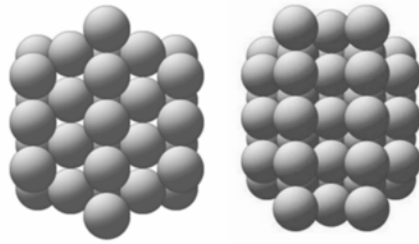


Fig 1.1

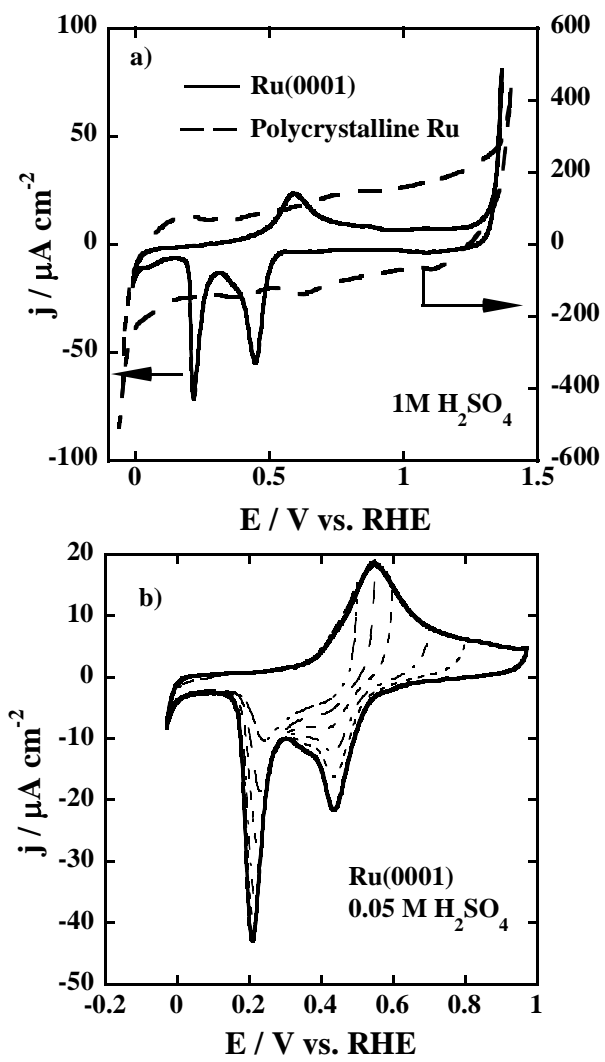


Fig. 3.1

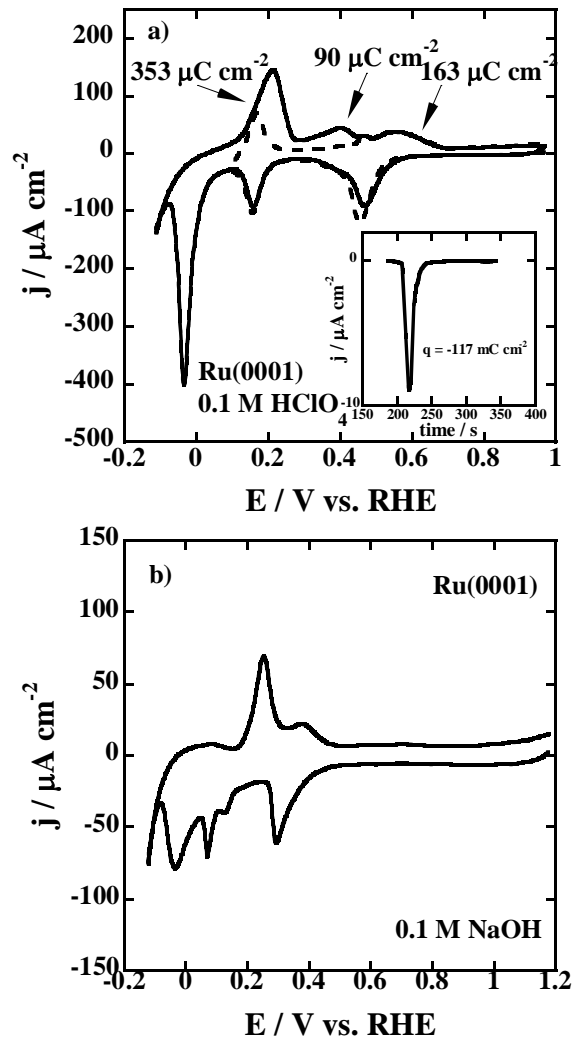


Fig. 3.2

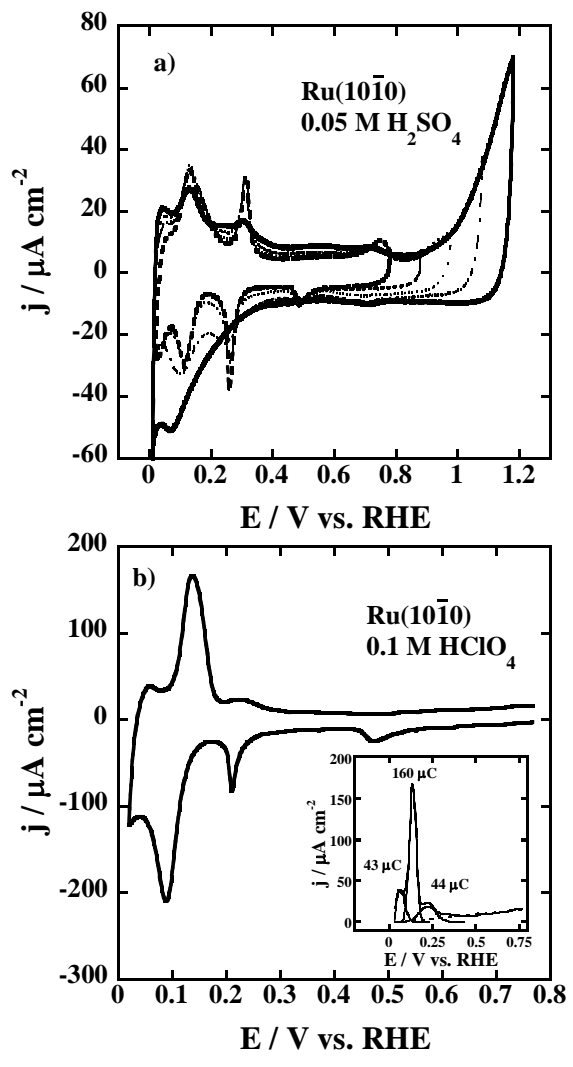


Fig. 3.3

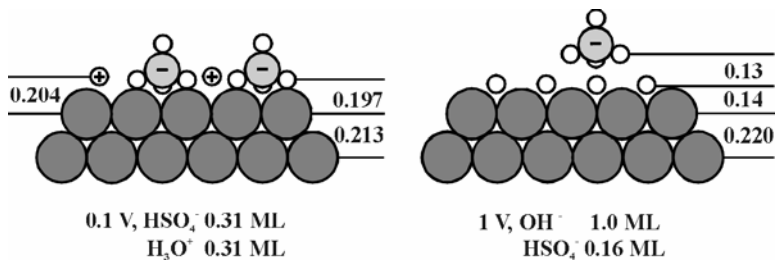


Fig. 3.4

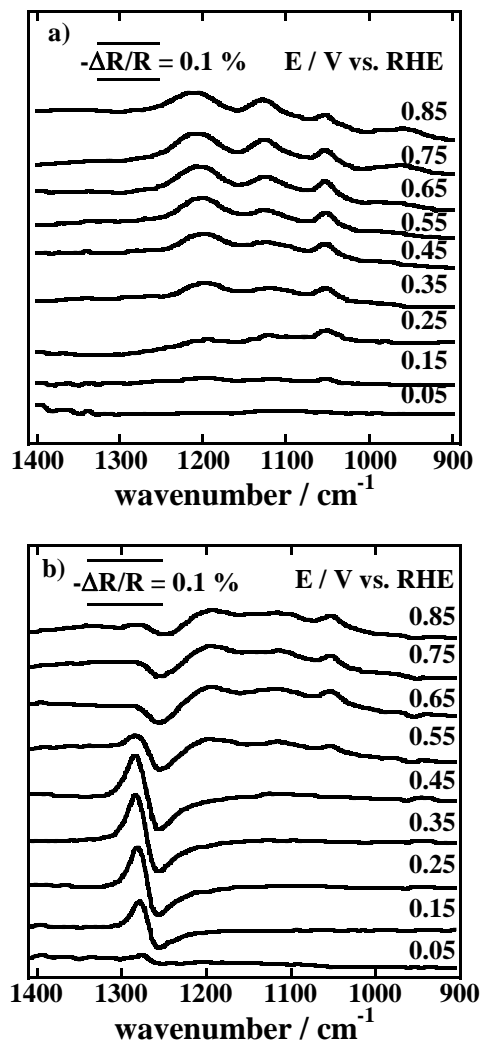


Fig. 3.5

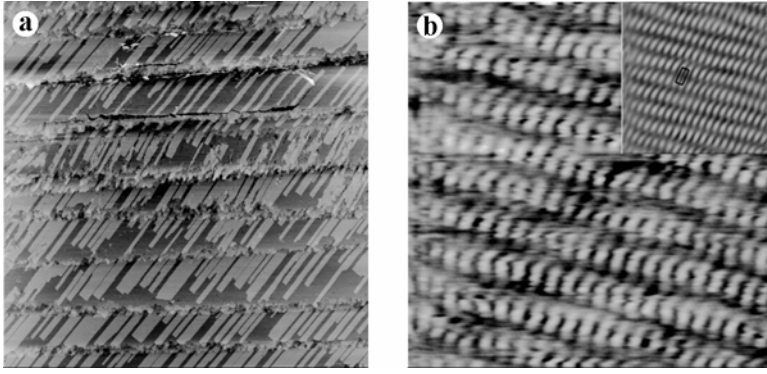


Fig. 3.6

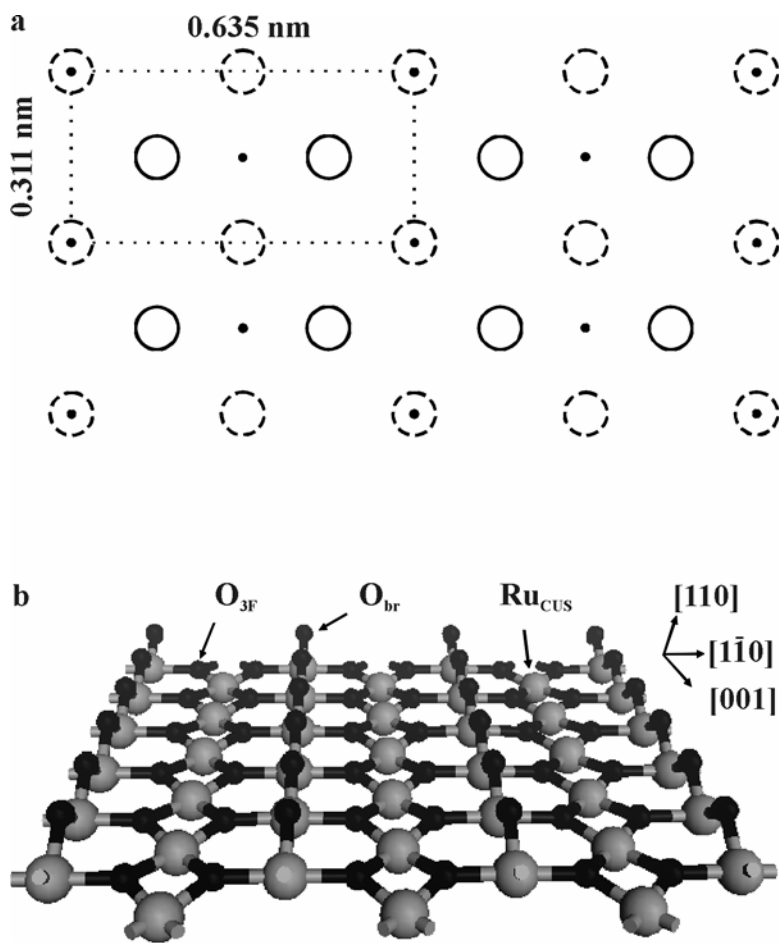


Fig. 3.7

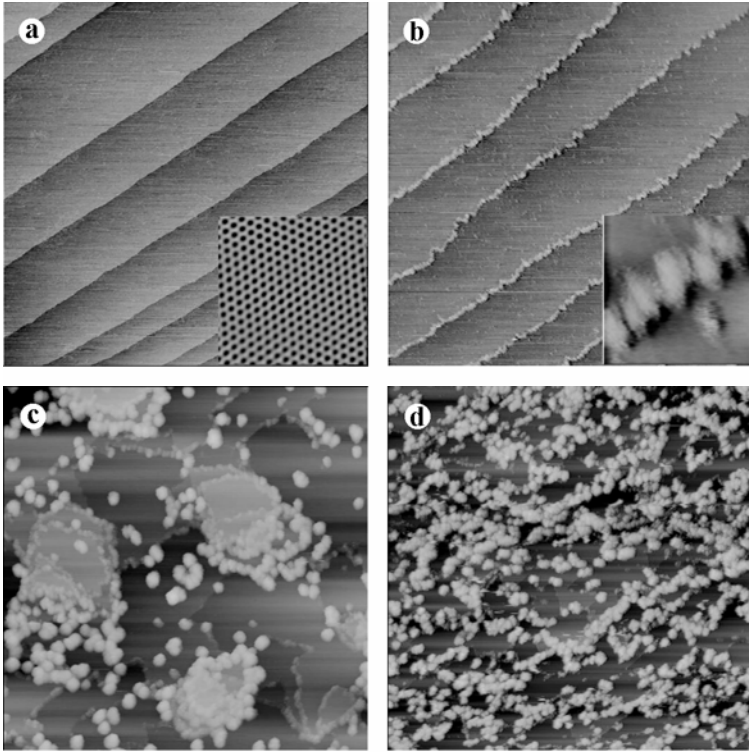


Fig. 3.8

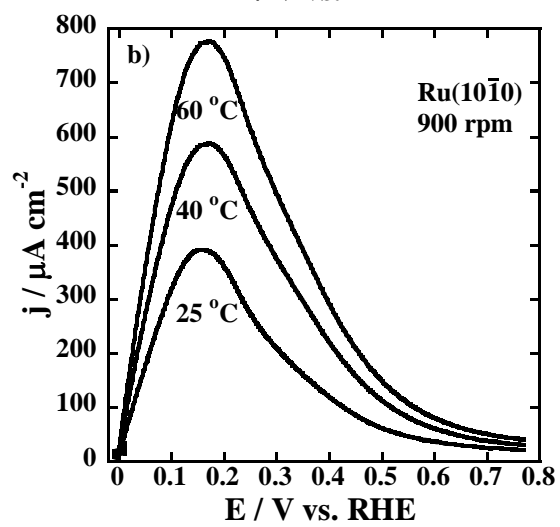
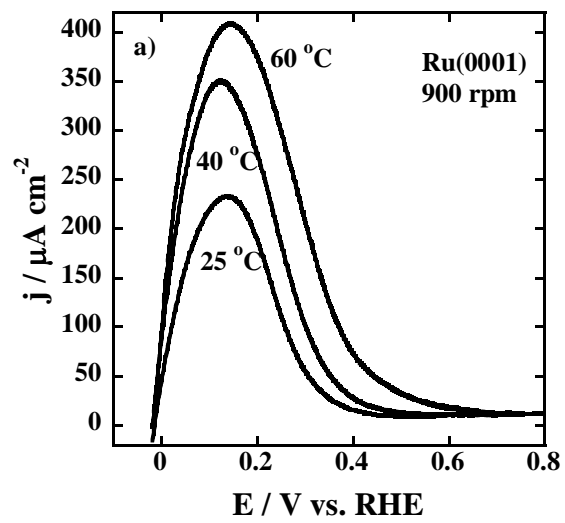


Fig. 4.1

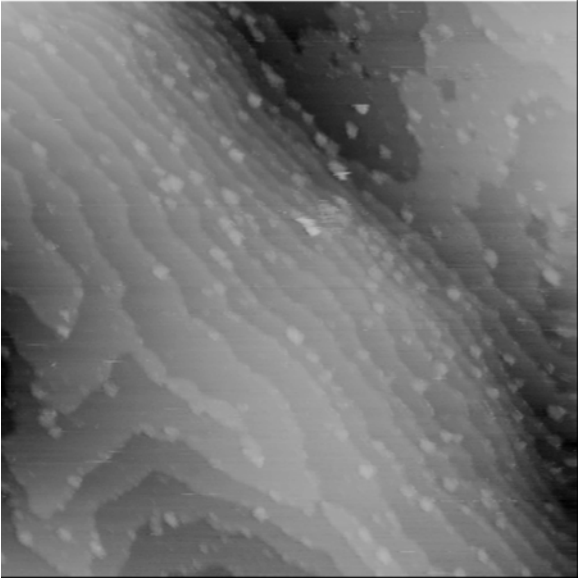


Fig. 4.2

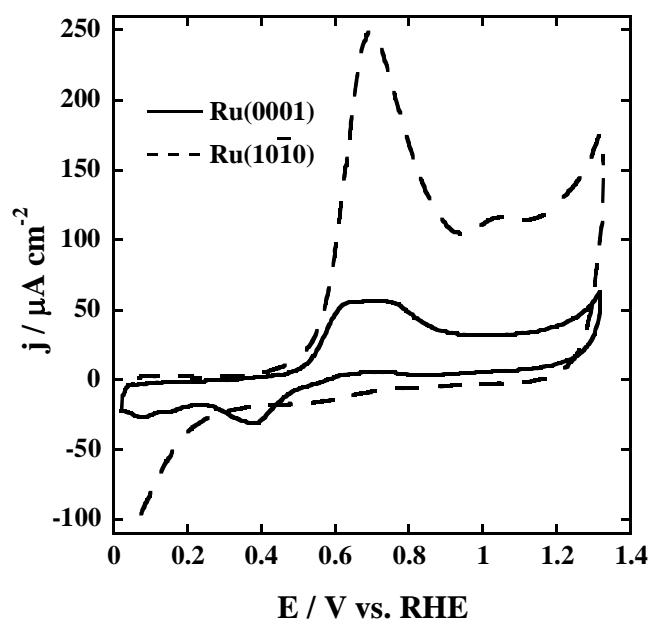


Fig. 4.3

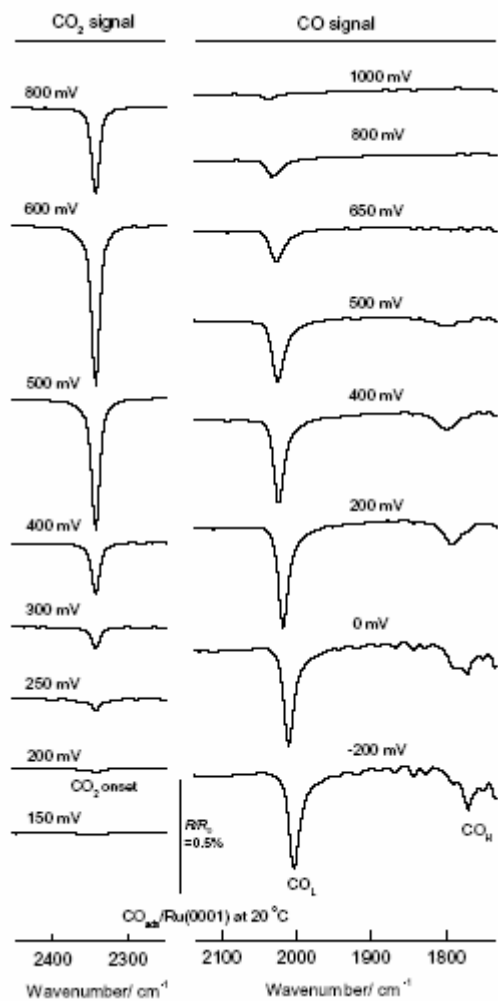


Fig. 4.4

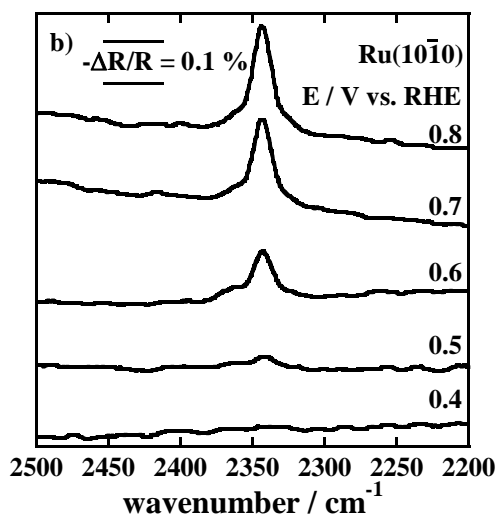
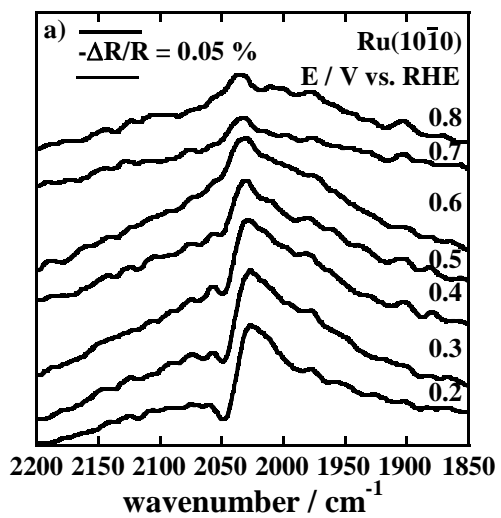


Fig. 4.5

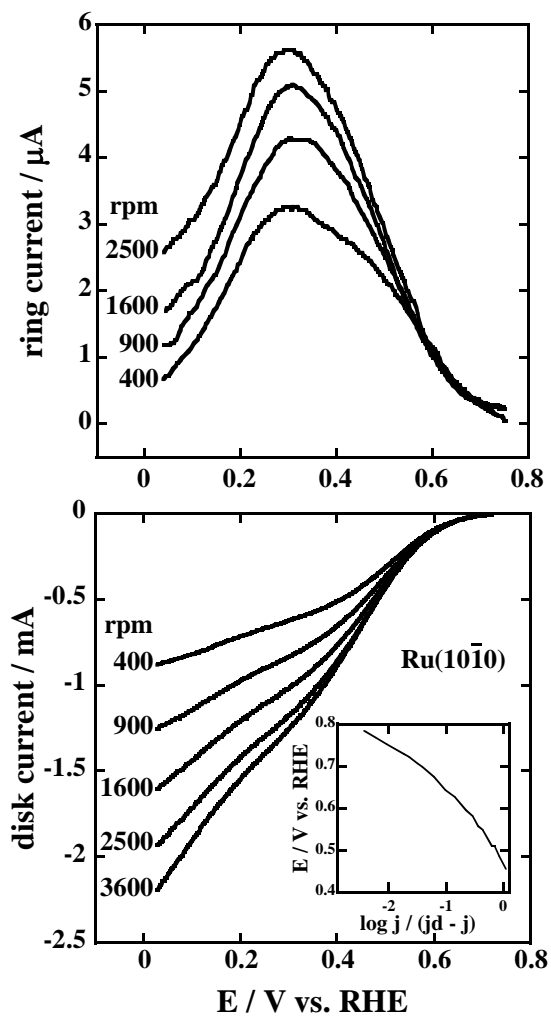


Fig. 4.6

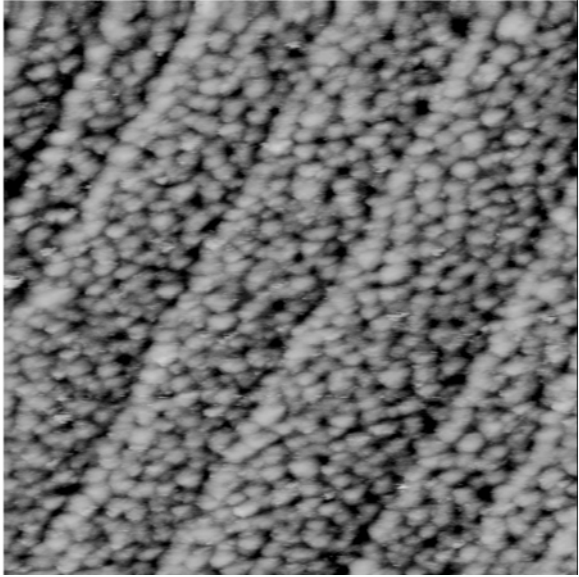


Fig. 5.1

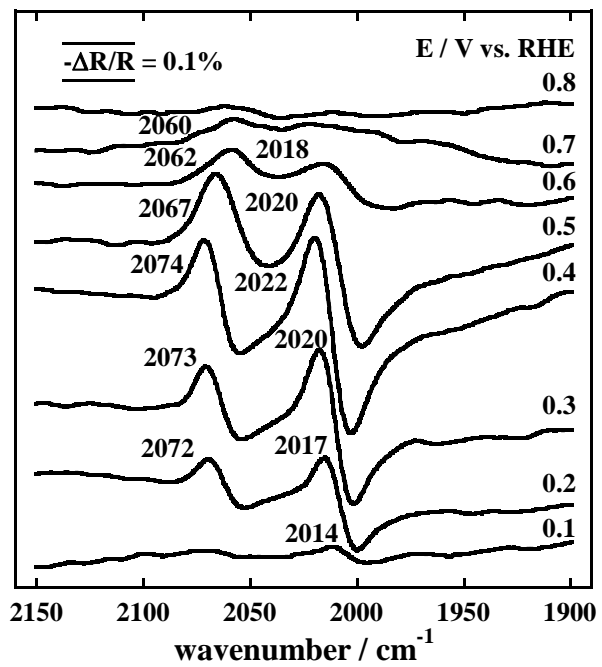


Fig. 5.2

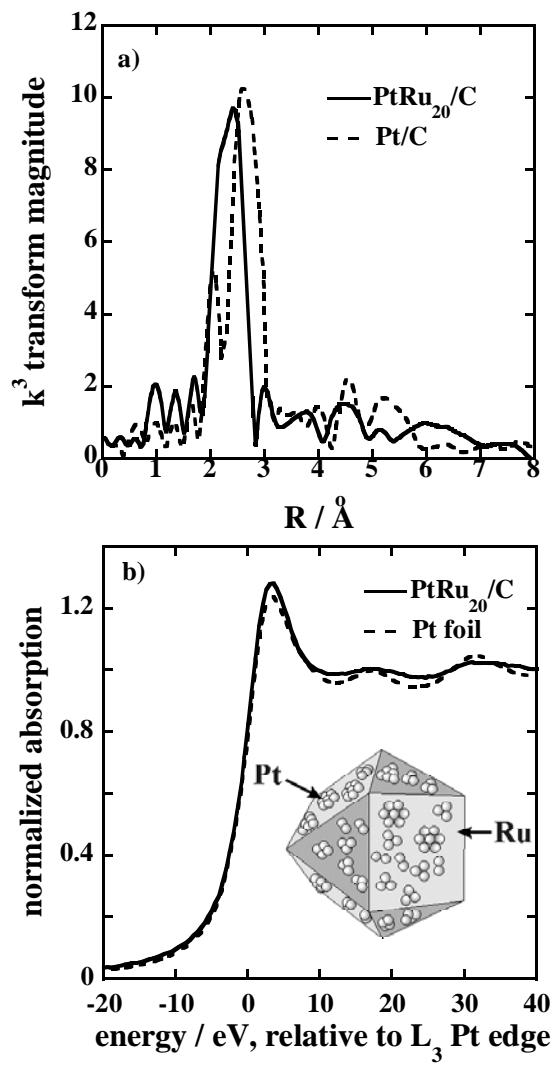


Fig. 5.3

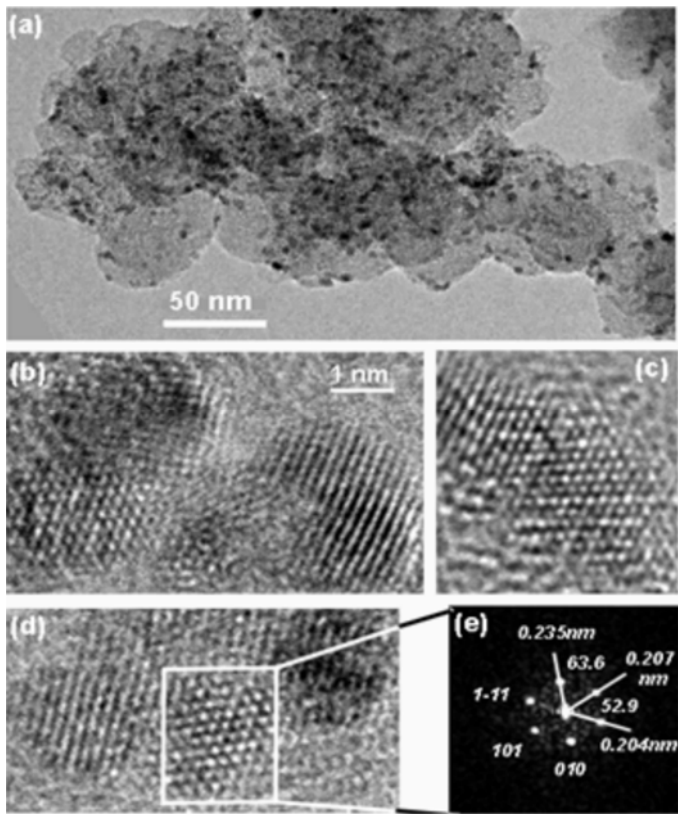


Fig. 5.4

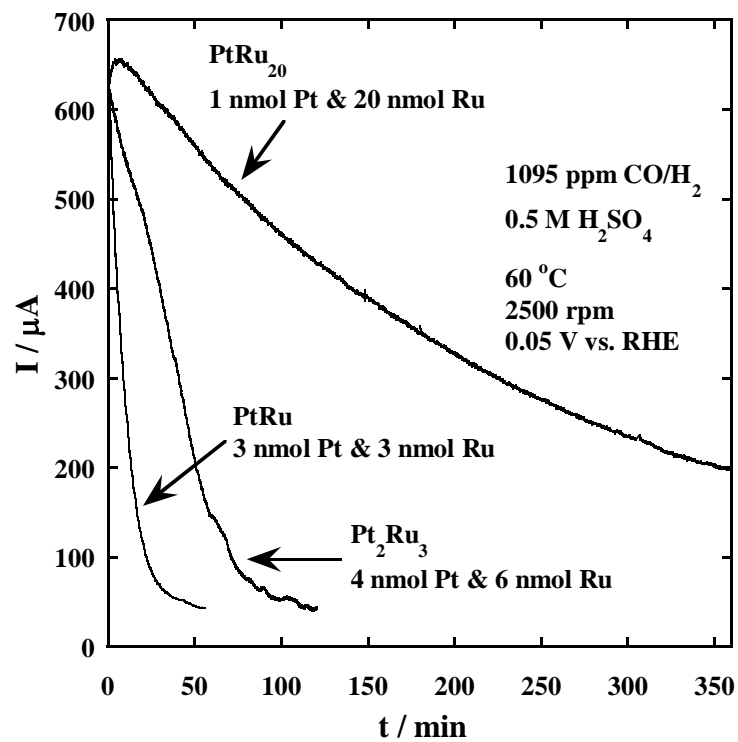


Fig. 5.5

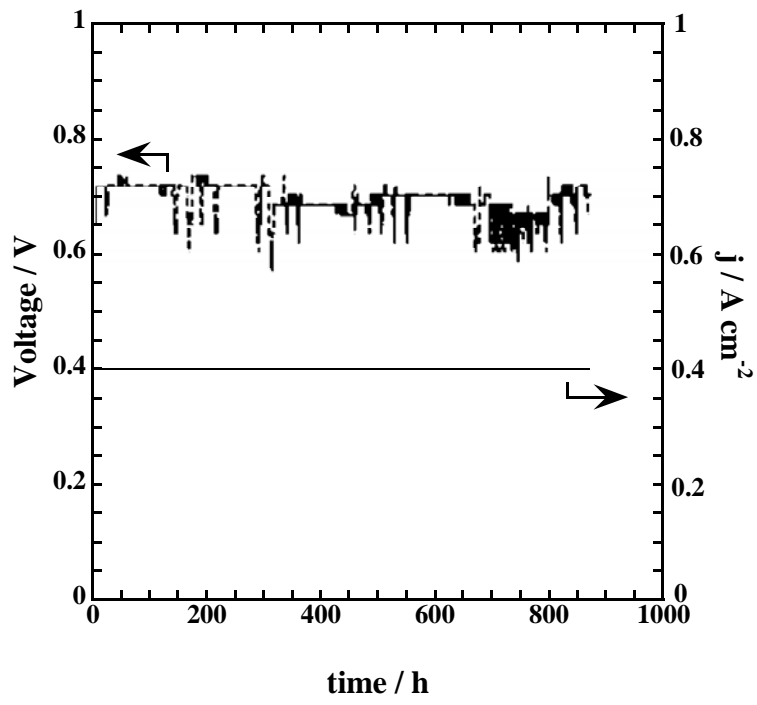


Fig. 5.6

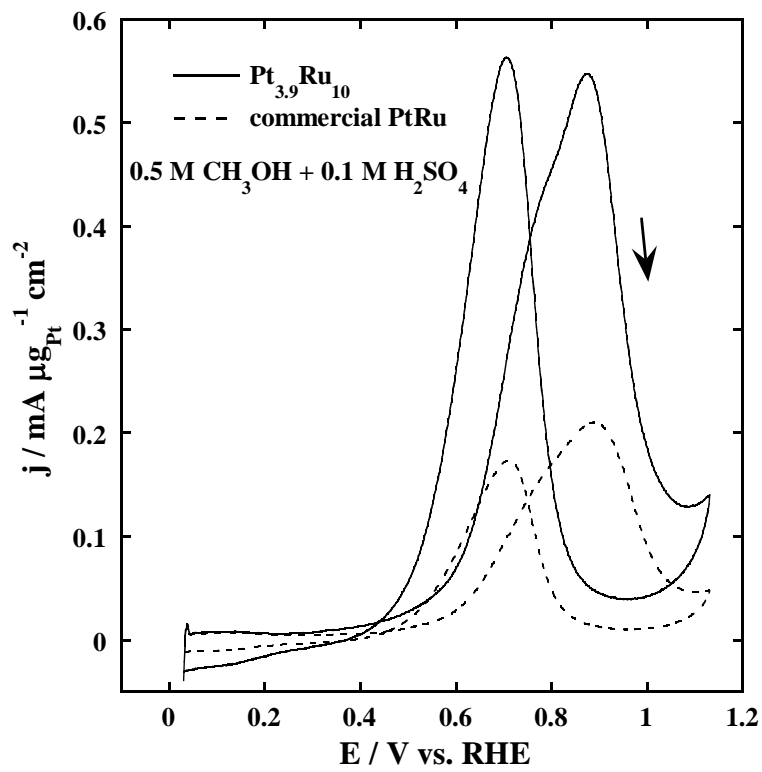


Fig. 5.7